Ore Geology Reviews 65 (2015) 1021–1042

Contents lists available at ScienceDirect

Ore Geology Reviews

journal homepage: www.elsevier.com/locate/oregeorev

Constraints of *in situ* zircon and cassiterite U–Pb, molybdenite Re–Os and muscovite ^{40}Ar–^{39}Ar ages on multiple generations of granitic magmatism and related W–Sn mineralization in the Wangxianling area, Nanling Range, South China

Rong-Qing Zhang [a], Jian-Jun Lu [a,*], Ru-Cheng Wang [a], Ping Yang [b], Jin-Chu Zhu [a], Yuan Yao [c], Jian-Feng Gao [d], Chao Li [e], Ze-Heng Lei [f], Wen-Lan Zhang [a], Wei-Min Guo [c]

[a] State Key Laboratory for Mineral Deposits Research, School of Earth Sciences and Engineering, Nanjing University, Xianlin University Town, 210023 Nanjing, China
[b] Geological Institute of Yunnan Nonferrous Geological Bureau, 650216 Kunming, China
[c] Nanjing Institute of Geology and Mineral Resources, CGS, 210016 Nanjing, China
[d] Geological Survey of Canada, Ottawa, ON K1A 0E8, Canada
[e] National Research Center of Geoanalysis, 26 Baiwanzhuang, 10037 Beijing, China
[f] Southern Hunan Institute of Geology and Survey, 423000 Chenzhou, China

ARTICLE INFO

Article history:
Received 30 March 2014
Received in revised form 13 September 2014
Accepted 16 September 2014
Available online 28 September 2014

Keywords:
Zircon U–Pb age
molybdenite Re–Os age
cassiterite U–Pb age
muscovite ^{40}Ar–^{39}Ar age
W and Sn mineralization
Wangxianling
Nanling Range
South China

ABSTRACT

The Nanling Range in South China hosts numerous W–Sn–rare metal deposits associated with several cycles of polygenetic granitic intrusions. In the Wangxianling area of the middle Nanling Range, igneous intrusions include the Wangxianling and Hehuaping granite plutons and more than 20 granite porphyry dykes. The Wangxianling pluton has a central phase of medium-grained tourmaline two-mica granite and a marginal phase of medium-grained tourmaline muscovite granite. The pluton hosts several tungsten deposits including Shuiyuanshan and Yejiwo. Mineralization type is dominantly scheelite greisen, with subordinate scheelite skarn and wolframite–quartz veins. The Hehuaping pluton composed of coarse-grained biotite granite and granite porphyry dykes to the east of the Wangxianling pluton have an associated Hehuaping tin deposit with tin skarn and subordinate porphyry and greisen mineralization.

In situ zircon and cassiterite U–Pb dating, molybdenite Re–Os and muscovite ^{40}Ar–^{39}Ar dating techniques are used to refine the age spectra of granitic rocks and W–Sn mineralization in the Wangxianling area. Granites of the Wangxianling pluton have zircon U–Pb ages of ~224 Ma. Tungsten-bearing quartz veins from both the Shuiyuanshan and Yejiwo tungsten deposits have an average molybdenite Re–Os isochron age of ~224 Ma, and muscovite of scheelite greisen from the Shuiyuanshan tungsten deposit yields a ^{40}Ar–^{39}Ar plateau age of 214 Ma. The two mineralization ages are consistent with the zircon U-Pb age of the Wangxianling pluton indicating a close association between pluton emplacement and W mineralization in the Late Triassic. Both the Hehuaping pluton and granite porphyry dykes have zircon U–Pb ages of ~156 Ma. *In situ* LA–ICP–MS U–Pb dating of cassiterite in both the tin skarn and tin greisen yields an average age of ~156 Ma, showing that the Sn mineralization occurred at a similar time to the Late Jurassic granitic magmatism. Thus, two mineralization events are identified in the Wangxianling area, and include an earlier W dominant mineralization event and a later Sn dominant mineralization event. The earlier event is related both spatially and temporally to intrusion of the Late Triassic S-type Wangxianling granite pluton, whereas the later mineralization is associated both spatially and temporally with intrusion of the Late Jurassic Hehuaping A_2-type granite pluton and A_2-type granite porphyry dykes.

1. Introduction

Precise and accurate isotopic dating is crucial for constraining the timing and genesis of mineral deposits. However, it is often difficult to obtain the reasonable ages of ore minerals directly due to the lack of suitable minerals for conventional radiometric dating. Actually, some modern dating techniques including U–Pb, ^{40}Ar–^{39}Ar, Re–Os and

* Corresponding author at: School of Earth Sciences and Engineering, Nanjing University, Xianlin University Town, 210023 Nanjing, China. Tel.: +86 025 83596605; fax: +86 025 83686016.
E-mail address: lujj@nju.edu.cn (J.-J. Lu).

http://dx.doi.org/10.1016/j.oregeorev.2014.09.021
0169-1368/

Sm–Nd isotope systems, are tested to constrain the temporal relationship between igneous intrusion and associated hydrothermal mineralization. As a common accessory mineral in granitic rocks, zircon is considered an essential and widely useful target for *in situ* U–Pb dating by LA-ICP-MS or SIMS (Jackson et al., 2004; Yuan et al., 2004). Muscovite ^{40}Ar–^{39}Ar dating is also a useful technique in determining the timing of hydrothermal mineralization particularly related to greisen or quartz vein (Mao et al., 2006a; Peng et al., 2006; Snee et al., 1988). Several other dating methods for ore minerals include Re–Os dating of molybdenite (Peng et al., 2006; Selby and Creaser, 2001; Selby et al., 2002; Stein et al., 2001), U–Pb and ^{40}Ar–^{39}Ar dating of cassiterite (Bai et al., 2013; Gulson and Jones, 1992; Yuan et al., 2008, 2011), U–Pb dating of columbite–tantalite (Che et al., 2014; Romer and Smeds, 1994; Romer and Wright, 1992; Romer et al., 1996), U–Pb dating of hübnerite (Romer and Lüders, 2006), U–Pb dating of uraninite (Luo et al., 2014), Sm–Nd dating of scheelite (Bell et al., 1989; Kempe et al., 2001) and U–Th–He dating of gold (Cabral et al., 2013). Therefore, using a multi-isotope dating approach, involving precise direct and indirect dating methods can provide comprehensive information about magmatic and hydrothermal systems related to the mineralization.

In the Nanling Range of South China, W–Sn–Mo–Bi mineralization may be associated with polygenetic granitic intrusions (Hu and Zhou, 2012; Mao et al., 2006b, 2013). During the past three decades, both tungsten- and tin-bearing granites in South China are generally considered to be transformation-series (or S-type) granites (Xu et al., 1982). Their differences have been highlighted in recent studies (Chen et al., 2008, 2013; Lu et al., 2011, 2012). The multiple episodes, Neoproterozoic to Cretaceous, of W and Sn mineralization in South China have been established (Mao et al., 1995). Even so, the refined genetic relations between ore-bearing granites and ore deposits remain unclear in most areas, which have raised debates on the timing of mineralization. Undoubtedly, these issues are difficult to settle if precise ages of the ore deposits cannot be determined.

The Wangxianling pluton is located in the middle Nanling Range, and several tungsten and tin deposits (W deposits: Shuiyuanshan, Yejiwo; Sn deposit: Hehuaping) are found in the area. It was dated as a Mesozoic granite, first based on muscovite K–Ar ages (206.4–222.5 Ma) (Geologic Team of Southern Hunan Province, 1983), and then confirmed by later zircon U–Pb ages (212 Ma, Wei et al., 2007; 235 Ma, Zheng and Guo, 2012). Cai et al. (2006) obtained a molybdenite Re–Os isochron age of 226 Ma of the skarn-type tungsten deposit in the periphery of the pluton and they simply considered this age also to represent the timing of Sn mineralization of the Hehuaping tin deposit. However, there are more than 20 Jurassic granite porphyry dykes near this tin deposit. Consequently, several questions may be raised: is there a hidden Jurassic granite pluton beneath the Hehuaping tin deposit? Is the tin mineralization related to Jurassic granite, rather than to Late Triassic one? Are there two episodes of magmatisms and two different types of mineralization in the Wangxianling area? In this study, a multi-dating approach is employed for both granitic rocks and W–Sn ores. The dating methods include *in situ* LA–ICP–MS zircon and cassiterite U–Pb dating, molybdenite Re–Os and muscovite ^{40}Ar–^{39}Ar dating. On the basis of the new dates obtained, we will discuss the genetic relationship between granitic magmatism and W–Sn mineralization in the Wangxianling area.

2. Geological background

The Nanling Range in South China (111°–117°E, 23°20'–26°40'N) covers a total area of 200,000 km^2 (Shu, 2007). In this region, there are strongly folded and deformed basement, and widespread granitoid intrusions and rifting basins. The basements are composed of a metamorphosed Neoproterozoic–Ordovician flysch–volcanic series and non-metamorphosed Late Devonian to Early Triassic sedimentary rocks (Wang and Shu, 2012). The granitoids formed from multiple cycles of tectono-magmatism. They are commonly directly associated with W–Sn–rare metal mineralization that defines the Nanling metallogenic belt is one of the 19 important metallogenic targets in China (Chen et al., 2013). Previous studies indicate that the W and Sn mineralization in the Nanling Range and its vicinity occurred from the Neoproterozoic, through the Paleozoic to the Mesozoic (Hu and Zhou, 2012; Mao et al., 1995, 2013). Over this long time span, the Jurassic and Cretaceous epochs are economically most important (Fig. 1). In the Wangxianling area of the middle Nanling Range, Mesozoic igneous activities have generated the Wangxianling granite pluton, the hidden Hehuaping granite pluton and granite porphyry dykes (Fig. 2).

2.1. Intrusive rocks

2.1.1. Wangxianling pluton

The Wangxianling granite pluton is exposed over an area of 19.7 km^2 and comprises the central and marginal phases (Fig. 2), both of which have similar mineral assemblages, textures and chemical compositions. The central phase consists dominantly of quartz (~36%), K-feldspar (~27%), plagioclase (~28%), tourmaline (~3%), biotite (~2%) and muscovite (~3%), and similarly the marginal phase mainly comprises quartz (~35%), K-feldspar (~28%), plagioclase (~27%), tourmaline (~4%) and muscovite (~5%) (Fig. 3a–d). Magmatic muscovite and tourmaline are common but are more abundant in the marginal phase than in the central phase. Accessory minerals are zircon, apatite, monazite, thorite, rutile and xenotime. Greisenization and sericitization are extensive, with pyrite, fluorite, scheelite, wolframite and arsenopyrite occurring in the alteration zone. The mineralization styles associated with the Wangxianling pluton are predominantly scheelite greisen, with subordinate quartz–wolframite vein and scheelite skarn.

Major and trace elements for granites in the Wangxianling area are given in Table 1. Rocks of the Wangxianling granite pluton have high Al_2O_3 (14.45 wt%) and P_2O_5 (0.19 wt%), and average Li, Th, Y and Zr + Nb + Ce + Y concentrations are 169, 16.4, 14.6 and 153 ppm, respectively. There are negative correlations between P_2O_5, Th and Y vs. SiO_2. The rocks have low REE abundances (88.2 ppm on average), with average LREE and HREE contents of 78.8 ppm and 9.4 ppm, respectively. They have initial $^{87}Sr/^{86}Sr$ ratios of 0.7202 to 0.7314, $\varepsilon_{Nd}(t)$ values of −10.3 to −14.4 and *in situ* zircon $\varepsilon_{Hf}(t)$ values of −4.1 to −18. The corresponding two-stage Nd and Hf model ages are 1.84–1.95 Ga and 1.75 Ga (peak value), respectively. Inherited zircons are common in the granite, and the average zircon saturation temperature is 739 °C. All of the above chemical and isotopic compositions illustrate that the Wangxianling pluton is a S-type granite.

2.1.2. Hehuaping pluton

The Hehuaping pluton in the Hehuaping tin deposit is a coarse-grained biotite granite. The pluton is mostly hidden but is observed in many drill holes below ground surface of ~280 m. It is also locally exposed in the southeastern periphery of the Wangxianling pluton (Fig. 2). At shallower depths, the Hehuaping biotite granite may be fine-grained and subjected to intensive greisenization. Previously this granite was considered to be a part of the Wangxianling pluton (Geologic Team of Southern Hunan Province, 1983). However, the biotite granite has mineralogical, petrographical and geochemical features that are distinctly from those of the Wangxianling granite. The Hehuaping granite consists primarily of quartz (~37%), K-feldspar (~35%), plagioclase (~21%) and biotite (~5%) (Fig. 3e, g). Accessory minerals include zircon, thorite, monazite, apatite and rutile. The tin greisen and tin skarn (cassiterite–sulfide) are spatially associated with the Hehuaping pluton.

Compared with granites from the Wangxianling pluton (Table 2), rocks of the Hehuaping pluton have high Th (51.4 ppm), Zr + Nb + Ce + Y (394 ppm) and total REE (346 ppm) contents. It has low LREE/HREE ratios and strongly negative Eu anomalies. These granite samples have relatively low initial $^{87}Sr/^{86}Sr$ ratios (0.7098 to 0.7264), high

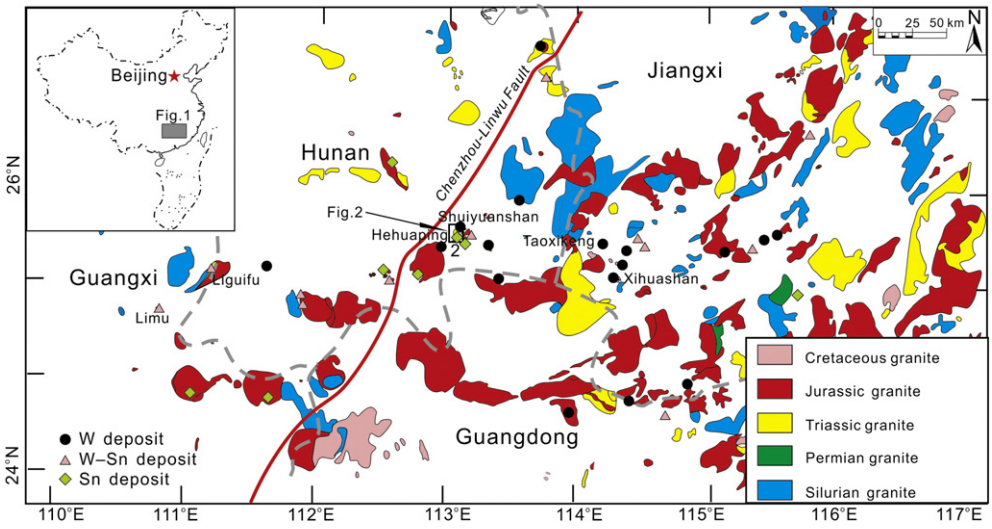

Fig. 1. Sketch map showing the granitic rocks of different ages and related W, W–Sn and Sn deposits in the Nanling Range (modified after Zhou et al., 2006).

$\varepsilon_{Nd}(t)$ values (−5.1 to −7.3) and young Nd isotopic model ages (1.36–1.54 Ga). The *in situ* $\varepsilon_{Hf}(t)$ values of zircons range from −0.9 to −9.6, with a two-stage model age of 1.55 Ga (peak value). Inherited zircon is rare in the Hehuaping biotite granite, which is consistent with the high zircon saturation temperature of 794 °C. The geochemical signatures indicate that the Hehuaping biotite granite is A_2-type.

2.1.3. Granite porphyry dykes

To the Southeast of the Wangxianling pluton, there are more than 20 NNE- and NE-trending granite porphyry dykes (Fig. 2), which intrude the Hehuaping biotite granite (Fig. 3f). The dykes are 200–1000 m long and 15–80 m wide, dipping southeast between 50° and 70°. Fresh porphyry dykes are grayish to pink, but altered dykes are grayish yellow. Granite porphyry dykes contain phenocrysts of quartz, K-feldspar, plagioclase and biotite (Fig. 3h); corrosion texture of high-temperature quartz, myrmekite and micrographic textures are common. Accessory minerals are zircon, monazite, rutile, apatite, titanite, ilmenite and magnetite. Spatially, the granite porphyry dykes are usually related to porphyry Sn–Bi mineralization.

Compared with the Wangxianling granite (Table 2), rocks of the granite porphyry dykes have low P_2O_5 (0.06 wt%), and high Th (71.0 ppm) and Zr + Nb + Ce + Y (395 ppm). Their REE, LREE and HREE contents are 305, 266 and 38.5 ppm, respectively. The dyke samples have initial $^{87}Sr/^{86}Sr$ ratios of 0.7079 to 0.7137, $\varepsilon_{Nd}(t)$ values of −7.2 to −8.0 and *in situ* zircon $\varepsilon_{Hf}(t)$ values of −2 to −14. The corresponding two-stage Nd and Hf model ages are 1.53–1.59 Ga and 1.65 Ga (peak value), respectively. The average zircon saturation temperature is 805 °C, and inherited zircon is rare in the granite porphyry dykes. The geochemical signatures indicate the granite porphyry dykes are A_2-type.

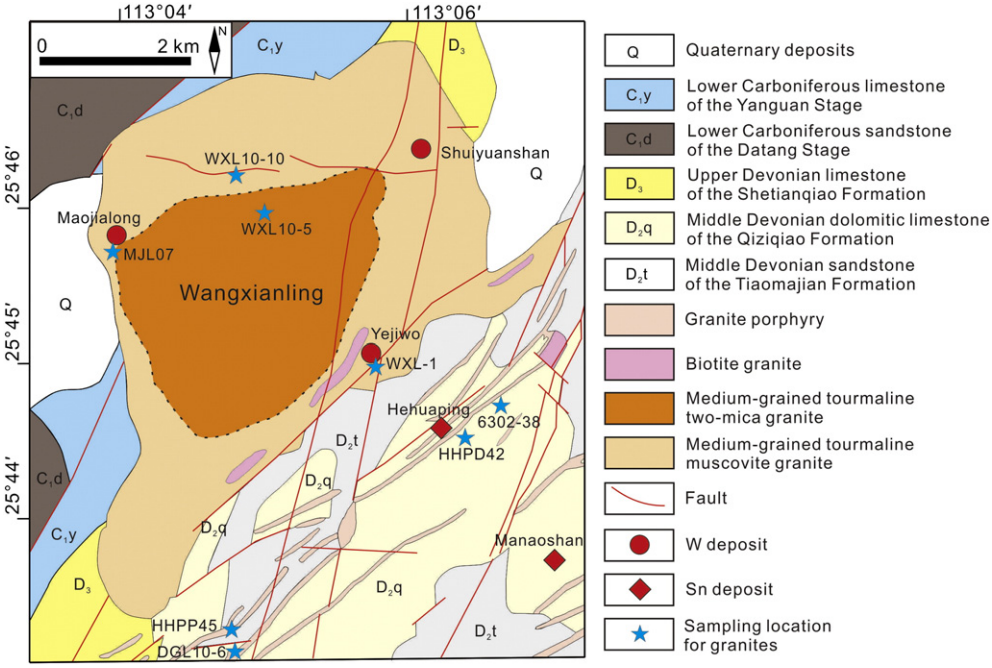

Fig. 2. Sketch map of the Wangxianling granite pluton (modified after Geologic Team of Southern Hunan Province, 1983).

2.2. Stratigraphy and fault structure

In the Wangxianling area, sedimentary rocks are Middle and Upper Devonian and Lower Carboniferous in age (Fig. 2). The Devonian sedimentary rocks can be divided into the Middle Devonian Tiaomajian and Qiziqiao formations, and the Upper Devonian Xikuangshan and Shetianqiao formations. The Tiaomajian Formation is up to 408 m thick and comprises gray quartz sandstone, siltstone and shale, with breccia-bearing sandstone and conglomerate beds at the base. The Qiziqiao Formation comprises mainly dolomitic limestone (lower part) and limestone (upper part) with a total thickness of more than 424 m. The Shetianqiao Formation, 285–305 m in thickness, comprises thick-bedded micritic limestone intercalated with thin-bedded, micritic and silty limestone. The Xikuangshan Formation is predominantly a massive chert-bearing limestone and dolomitic limestone, and is 398–458 m thick. The Lower Carboniferous sedimentary rocks are in conformable contact with the Devonian strata can be subdivided into the Yanguan and Datang stages. The Yanguan Stage, 538 m thick,

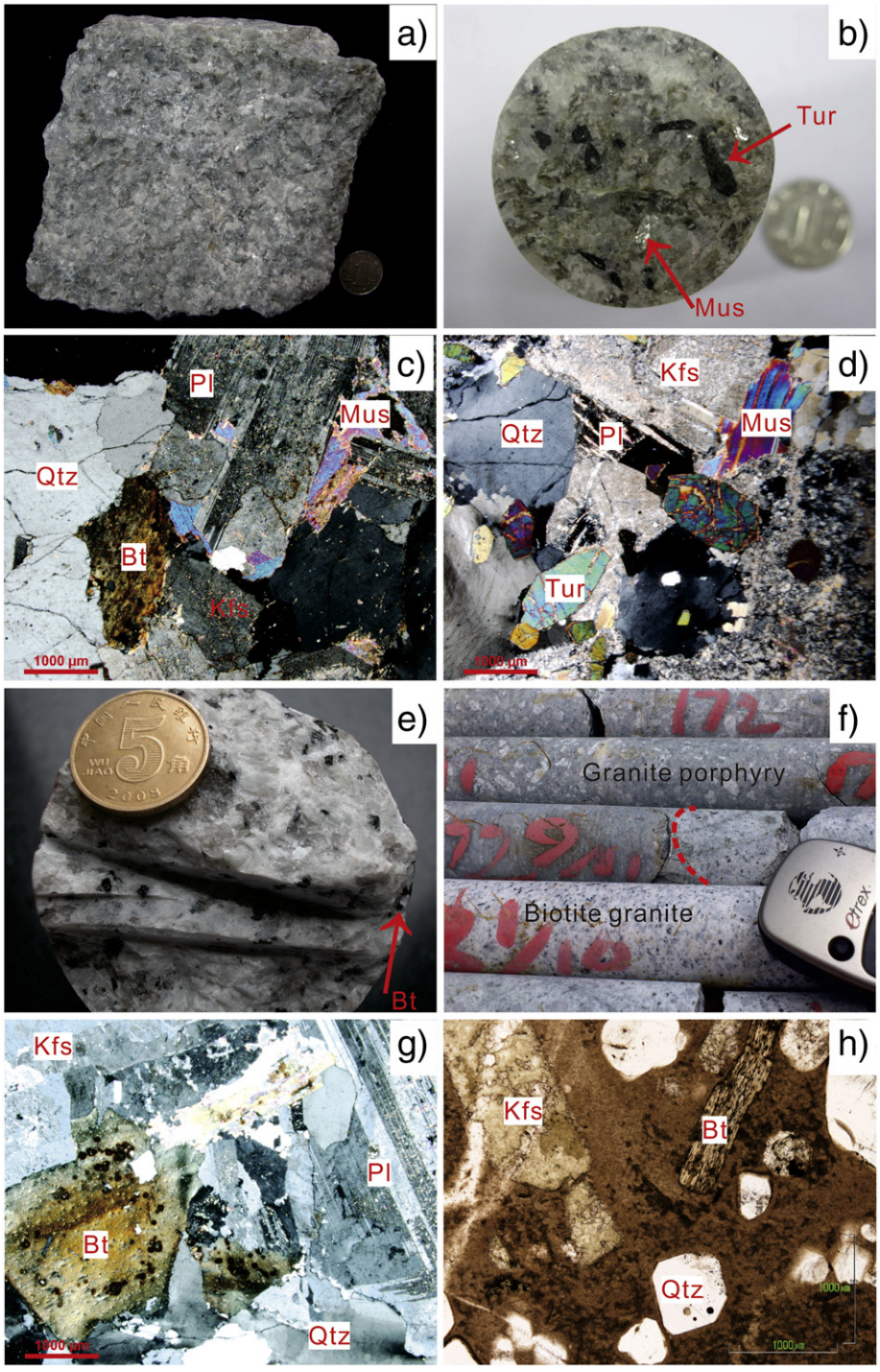

Fig. 3. Photographs and photomicrographs of granitic rocks in the Wangxianling area. (a) Medium-grained two-mica granite. (b) Medium-grained tourmaline muscovite granite. (c) Photomicrograph of medium-grained two-mica granite (crossed nicols). (d) Photomicrograph of medium-grained tourmaline muscovite granite (crossed nicols). (e) Coarse-grained biotite granite from drill hole ZK4701. (f) Contact, as marked by a red dash, between biotite granite and a granite porphyry dyke from drill hole ZK7907. (g) Photomircrograph of coarse-grained biotite granite from drill hole ZK4701 (crossed nicols). (h) Photomicrograph of a granite porphyry dyke from the Hehuaping tin deposit (plane light). Abbreviations: Pl (plagioclase), Qtz (quartz), Mus (muscovite), Bt (biotite), Kfs (K-feldspar), Tur (tourmaline).

Table 1
Chemical compositions of major (wt%) and trace elements (ppm) of the intrusive rocks in the Wangxianling area.

Rock type	Wangxianling tourmaline muscovite granite	Hehuaping biotite granite	Granite porphyry dykes	Rock type	Wangxianling tourmaline muscovite granite	Hehuaping biotite granite	Granite porphyry dykes
Elements	Mean (n=10)	Mean (n=10)	Mean (n=6)	Elements	Mean (n=10)	Mean (n=10)	Mean (n=6)
SiO_2	73.22	74.53	74.80	Zr	77.3	163	174
TiO_2	0.15	0.15	0.16	Hf	2.7	6.8	6.9
Al_2O_3	14.45	13.1	12.24	Y	14.7	65.7	61.5
Fe_2O_3	0.47	0.46	0.38	Ga	19.8	22.7	19.5
FeO	0.69	1.11	1.22	W	24.8	5.5	9.9
FeOt	1.12	1.53	1.56	Sn	20.1	13.7	19.8
Fe_2O_3t	1.24	1.7	1.73	La	18.6	66.7	63.5
MnO	0.06	0.03	0.04	Ce	37.8	140	129
MgO	0.37	0.13	0.43	Pr	4.1	16.1	14.1
CaO	0.90	1.13	1.23	Nd	14.1	60.9	48.63
Na_2O	3.17	2.93	1.72	Sm	3.1	12.8	10.2
K_2O	4.54	4.74	5.53	Eu	0.29	0.53	0.39
P_2O_5	0.19	0.04	0.06	Gd	2.8	12.6	9.8
LOI	1.51	1.17	1.95	Tb	0.48	2.2	21.7
Total	99.72	99.53	99.73	Dy	2.6	13.2	10.1
ACNK	1.24	1.09	1.11	Ho	0.47	2.7	2.0
ANK	1.43	1.32	1.44	Er	1.4	8.1	6.4
FeOt/MgO	3.04	12.93	5.15	Tm	0.22	1.2	0.98
Sc	5.6	5.2	3.5	Yb	1.3	7.6	6.5
V	10.0	5.2	6.7	Lu	0.19	1.1	0.98
Cr	4.3	9.8	8.6	Zr+Nb+Y+Ce	153	394	395
Co	1.5	1.0	1.4	total REE	88.2	346	305
Be	19.6	8.2	7.6	LREE	78.8	297	266
Li	169	52.0	28.1	HREE	9.4	48.7	38.5
Cs	116	19.0	23.3	LREE/HREE	8.3	7.0	7.1
Rb	422	385	550	10000*Ga/Al	2.59	3.29	3.02
Ba	144	143	137	K/Rb	90.0	113	84.8
Th	16.4	54.4	71.0	Rb/Sr	8.6	9.8	26.2
U	20.3	23.5	21.2	Nb/Ta	3.5	6.5	6.2
Nb	23.6	25.6	30.6	Zr/Hf	28.3	24.4	25.4
Ta	7.0	4.4	5.0	Th/U	0.9	2.5	3.6
Pb	31.9	32.8	72.4	La_N/Yb_N	9.4	7.7	6.9
Sr	65.1	55.2	29.8	T_{Zr} (°C)	739	794	805

consists of mainly marl, limestone, dolomitic limestone and subordinate siltstone and shale. The Datang Stage is 308–566 m thick and is primarily limestone and dolomite with lesser sandstone and shale in the middle part of the stage. Limestone of the Lower Carboniferous Datang Stage and the Upper Devonian Xikuangshan Formation is the dominant host rock of skarn- and greisen-type scheelite deposits. The dolomitic limestone of the Qiziqiao Formation is the predominant host rock for tin skarn.

Adjoining West of the Wangxianling area is the NE-striking Chenzhou–Lingwu fault (Fig. 1). This major fault controls the structural framework of the area. Smaller faults striking approximately NNE, NE and EW cut through the Wangxianling pluton (Fig. 2). The granite porphyry dykes are associated with the NE-striking faults whereas the Hehuaping pluton is controlled by deep-rooted NNE-striking faults.

2.3. Deposit geology

2.3.1. Tungsten deposits

Several tungsten deposits, such as Shuiyuanshan and Yejiwo, are located in the periphery of the Wangxianling pluton (Fig. 2). Scheelite greisen is the dominant ore type, followed by scheelite skarn and wolframite–quartz vein types. The total WO_3 reserve is more than 0.11 Mt.

The Shuiyuanshan tungsten deposit in the northeastern Wangxianling pluton consists of several scheelite greisens, and also has smaller-scale scheelite skarns and wolframite–quartz veins (Fig. 4). The scheelite greisen (Fig. 5a, b) is located as an alteration zone, about 600 m long, 400 m wide and 5–80 m thick, in the roof of the Wangxianling granite. Two small scheelite skarns are found at the contact between the northern Wangxianling granite and limestone of the Xikuangshan Formation. NNE- and NWW-striking wolframite–quartz veins crosscut the muscovite–tourmaline granite. Disseminated molybdenite flakes are common in these veins (Fig. 5c).

The Yejiwo tungsten deposit is located in the northern Wangxianling pluton, including several W-bearing tourmaline–quartz veins and scheelite skarns (Fig. 5d). The tungsten-bearing tourmaline–quartz vein can cut through the Wangxianling granite. Scheelite skarns are revealed by

Table 2
Comparison of the intrusive rocks in the Wangxianling area.

Rocks	Wangxianling tourmaline muscovite granite	Hehuaping biotite granite	Granite porphyry dykes
Genetic type	S-type	A_2-type	A_2-type
Magmatic tourmaline	Common	None	None
Magmatic muscovite	Common	None	None
Inherited zircon	Common	Rare	Rare
Al_2O_3 (wt%)	14.45	13.10	12.24
P_2O_5 (wt%)	0.19	0.04	0.06
Th (ppm)	16.4	51.4	71
W (ppm)	24.8	5.5	9.9
Sn (ppm)	20.1	13.7	19.8
Zr+Nb+Ce+Y (ppm)	153	394	395
REE (ppm)	88.2	346	305
LREE (ppm)	78.8	297	266
HREE (ppm)	9.4	48.7	38.5
T_{zr} (°C)	739	794	805
Initial Sr	0.720245 ~0.731391	0.709764 ~0.726389	0.707870 ~0.713761
$\varepsilon_{Nd}(t)$	−10.3~−14.4	−5.1~−7.3	−7.2~−8.0
T_{DM2} Nd (Ga)	1.84 ~1.95	1.36~1.54	1.53~1.59
$\varepsilon_{Hf}(t)$	−4.1~−18	0.9 ~−9.6	−2~−14
T_{DM2} Hf (Ga, peak value)	1.75	1.55	1.65

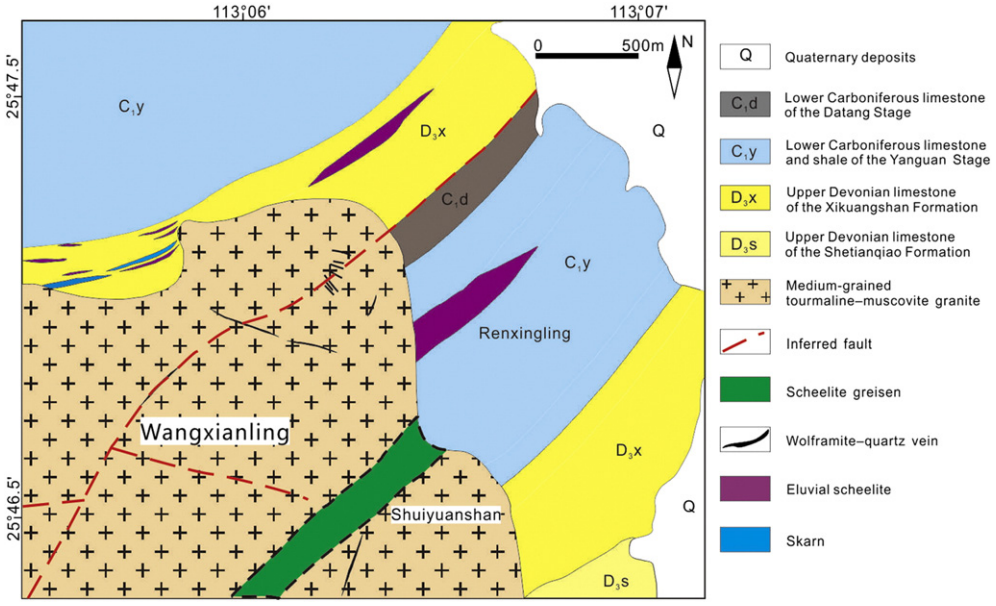

Fig. 4. Geological map of the Shuiyuanshan tungsten deposit.

drill holes between the contact of limestone of the Yanguan Stage (C_1y) and the Wangxianling pluton in its northwestern and southwestern peripheries.

2.3.2. Tin deposit

The Hehuaping tin deposit is located to the Southeast of the Wangxianling pluton (Figs. 2 and 6). Tin mineralization is spatially associated both with the hidden biotite granite pluton and granite porphyry dykes. The tin deposit consists of mainly skarn and subordinate porphyry and greisen ores. It has reserves of 27.4 Mt @ 0.72% Sn and commonly coexists with Pb, Zn (0.162 Mt Pb + Zn ore, @ 2.9% Pb and 3.5% Zn), and minor Mn and Bi mineralization.

There are five main orebodies in the Hehuaping tin deposit (Fig. 6). The largest of the orebodies, No. IV, occurs between dolomitic limestone of the Qiziqiao Formation and sandstone of the Tiaomajian Formation (Fig. 7). This orebody is related to a magnesian skarn system (~100 m in depth) with a mineral assemblage of forsterite, spinel, diopside, tremolite, serpentine, talc and phlogopite. A well-defined zoning is observed from the fresh coarse-grained biotite granite towards the limestone, beginning with greisenized granite, through quartz-rich greisen, quartz–fluorite vein bearing sericitized sandstone, cassiterite–magnetite skarn, forsterite–spinel–diopside skarn, serpentine–talc–phlogopite skarn, to cassiterite–sulfide bearing marble (Yao et al., 2014). The proximal skarn cassiterite–magnetite orebody is 3400 m

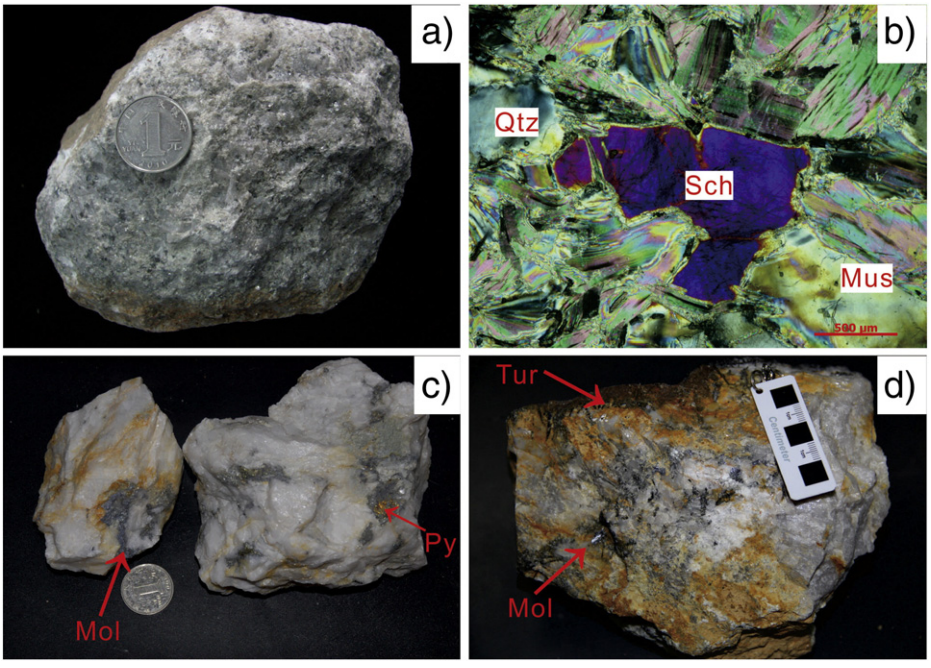

Fig. 5. Photographs and photomicrographs of tungsten ores from the tungsten deposits around Wangxianling pluton. (a) Scheelite greisen from the Shuiyuanshan tungsten deposit. (b) Photomicrograph of the scheelite greisen from the Shuiyuanshan tungsten deposit (crossed nicols). (c) Molybdenite-bearing wolframite–quartz vein from the Shuiyuanshan tungsten deposit. (d) Molybdenite- and scheelite-bearing tourmaline–quartz vein from the Yejiwo tungsten deposit. Abbreviations: Mol (molybdenite), Tur (tourmaline), Py (pyrite), Mus (muscovite), Qtz (quartz).

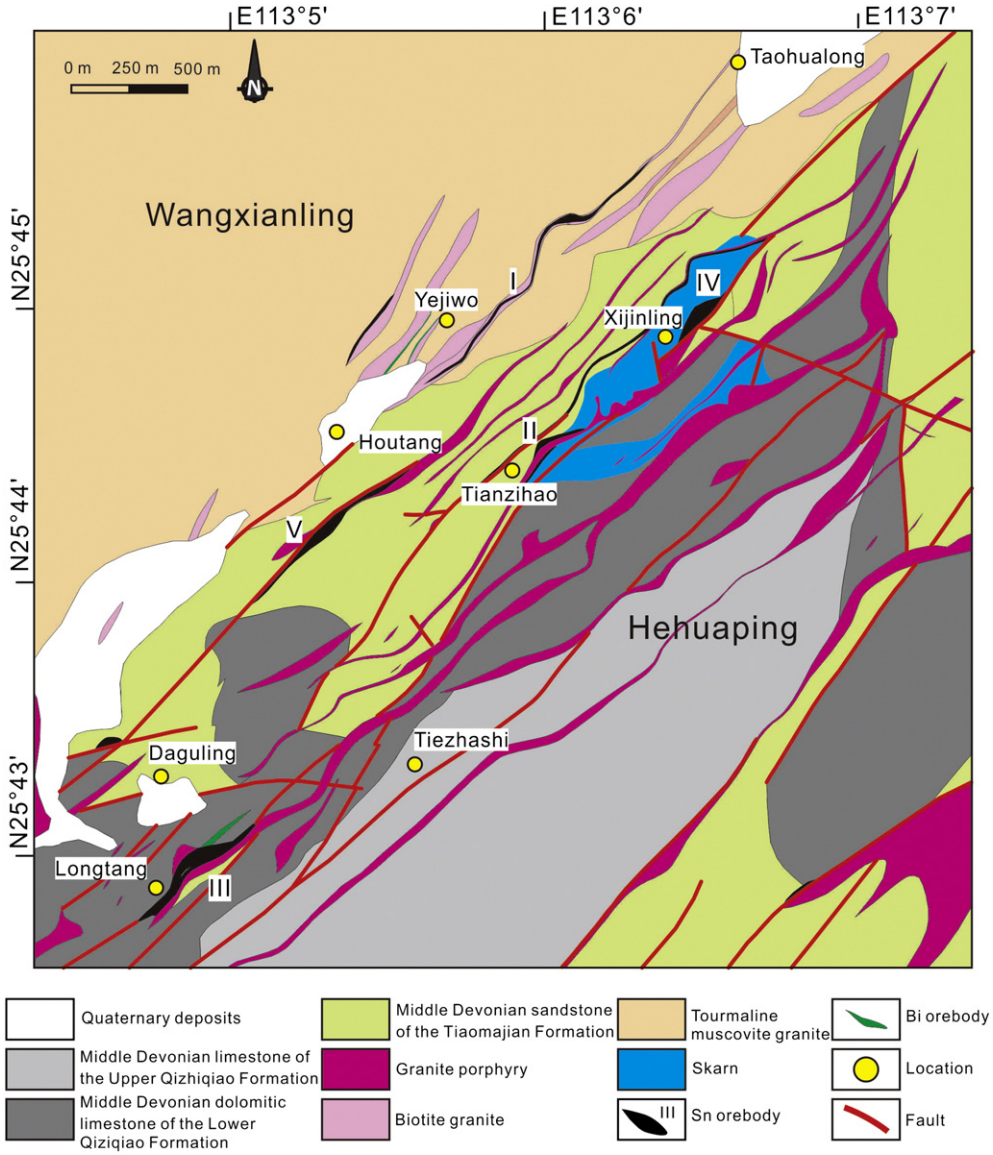

Fig. 6. Geological map of the Hehuaping tin deposit (modified after Wu, 2006).

long, 300–600 m wide and 5.01–16.09 m thick, and is strata-bound and sheet-like at the bottom of the skarn. Cassiterite grains coexisting with magnetite are very small (<100 μm) (Fig. 8a). In the distal skarn, cassiterite–sulfide veins are common and crosscut the marble (Fig. 8b, c). The cassiterite has a relatively large grain size (>100 μm) in these ores. In places, galena–sphalerite veins overprint the skarn and have grades of 0.15–3.19% Pb and 0.13–3.50% Zn.

The No. I and II orebodies are controlled by two NE-striking faults (Fig. 6). The cassiterite–sulfide ores occur in both the granite porphyry dykes and sandstone as disseminated and stockwork mineralization. The two orebodies are 150–1800 m long, 50–300 m wide and 1–21 m thick. The Sn, Pb and Zn reserves are 11.56 Mt @ 0.93%, 0.275 Mt @ 2.1% and 0.476 Mt @ 0.43%, respectively. Ore minerals include cassiterite, galena, sphalerite, bismuthinite, pyrite and arsenopyrite. The No. III and V tin orebodies, with an average grade of 0.51% Sn, are related to the granite porphyry dykes, and are 700–900 m long and 3.8–18 m thick. NE-striking porphyry dykes intrude into the dolomitic limestone of the Qiziqiao Formation and sandstone of the Tiaomajian Formation. Sericitization and silicification alteration is significant in the sandstone. Cassiterite–sulfide stockwork mineralization usually crosscuts the altered granite porphyry dykes and sandstone (Fig. 8d). Aside from the five main orebodies, three smaller Sn–Bi greisens (Fig. 8e) are found in the NE-striking Hehuaping fine-grained biotite granite in the eastern Hehuaping deposit. Brown to brownish black cassiterite grains occur as disseminated (200–500 μm) in the greisen (Fig. 8f).

3. Sampling and analytical procedures

3.1. In situ LA–ICP–MS zircon U–Pb dating

Eight granite samples were collected for selecting zircon grains, and their sampling locations are shown in Fig. 2. Sample WXL10-5 was collected from the central phase of the Wangxianling pluton, and samples WXL10-5, MJL07 and WXL-1 were from the marginal phase. Two samples of the hidden Hehuaping pluton (HHPD42 and 6302-38) were collected from two drill holes, ZK4701 and ZK6302, respectively. Two granite porphyry samples (HHPP45 and DGL10-6) were taken from two dykes in the southwestern Hehuaping tin deposit. After crushing the rock samples, zircons were separated using standard heavy liquid and magnetic separation techniques. Zircon grains were then handpicked under a binocular microscope, mounted in an epoxy resin disc and polished. Cathodoluminescence (CL) images were obtained using a JEOL JXA-8100 M electron microprobe at the State Key Laboratory for Mineral Deposits Research, Nanjing University, China.

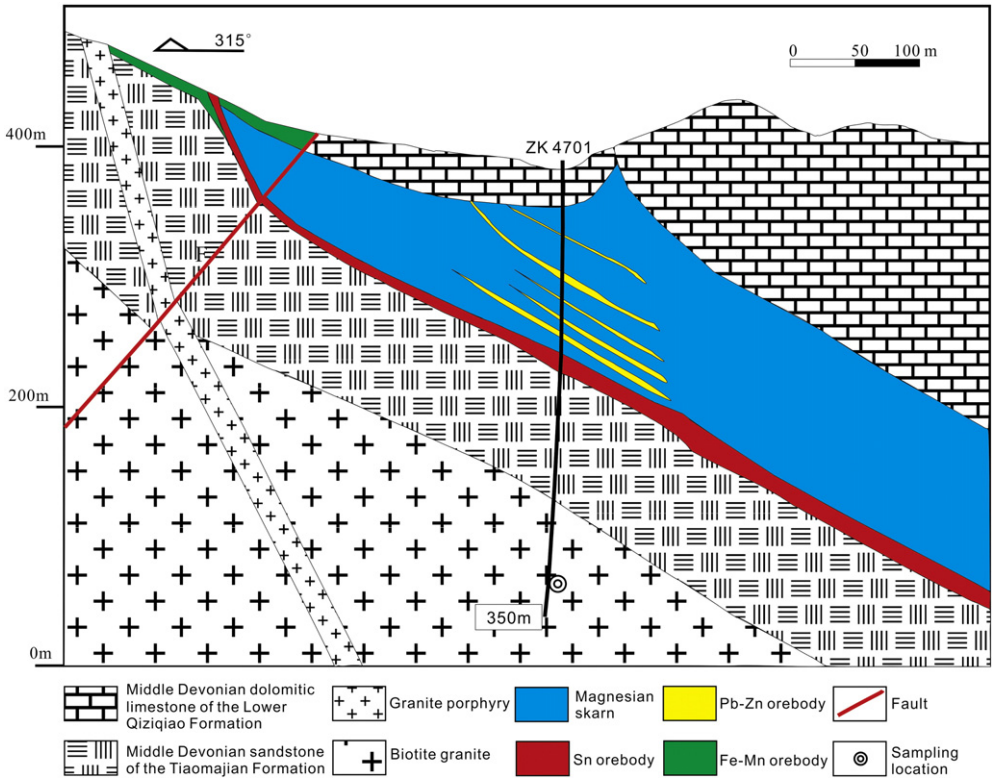

Fig. 7. Cross-section of the No. 47 exploration line in the Hehuaping tin deposit (modified after Wu, 2006).

Zircon U–Pb isotope analyses of two samples (HHPD42 and HHPP45) were undertaken by LA-ICP-MS at the Institute of Mineral Resources, Chinese Academy of Geological Sciences, Beijing, China. Detailed operating conditions for the laser ablation system and the MC-ICP-MS instrument, and data reduction protocols are the same as described by Hou et al. (2009). Zircon GJ1 (609 Ma; Jackson et al., 2004) was used as an external standard for U–Pb dating, and was analyzed twice every 5 to 10 analyses. Time-dependent drifts of U–Th–Pb isotopic ratios were corrected using a linear interpolation (with time) for every 5 to 10 analyses, according to the variations of GJ1. The zircon standard Plešovice was also used for quality control and yielded a weighted mean $^{206}Pb/^{238}U$ age of 337.4 ± 2.0 Ma (2σ, n = 6), which is in good agreement with the published $^{206}Pb/^{238}U$ age of 337.13 ± 0.37 Ma (2σ) (Sláma et al., 2008). Four samples (WXL10-5, WXL10-10, MJL07 and 6302-38) were measured on an Agilent 7500a ICP-MS equipped with a New Wave Research 213 Laser Ablation system at the State Key Laboratory for Mineral Deposits Research, Nanjing University, following He et al. (2010). Analyses were carried out using a beam diameter of 25 μm, 5 Hz repetition rate, and energy density of 18 J/cm^2. The GJ-1 was used as an external standard. Detailed analytical procedures are similar to those described by Jackson et al. (2004). Samples were analyzed in runs of approximately 18 analyses, which included 10 to 12 unknowns, bracketed by two to four analyses of the standard. The unknowns included zircon standard Mud Tank (TIMS age = 732 ± 5 Ma; Black and Gulson, 1978) which was analyzed as an independent control on reproducibility and instrument stability. ICP-MS data were reduced using the Glitter software, which yielded additional parameters such as isotope ratios, age, error, and Th and U contents. U-Pb ages of zircon for samples WXL-1 and DGL10-6 were obtained by LA-ICP-MS at the State Key Laboratory of Ore Deposit Geochemistry, Institute of Geochemistry, Chinese Academy of Sciences, Guiyang, China. A Lamda Physik GeoLasPro 193 nm ArF excimer laser-ablation system coupled with Agilent 7700× ICP-MS were used for the analyses. Analyses were carried out using a beam diameter of 32 μm at 5 Hz repetition rate and energy density of 10 J/cm^2 for 40 seconds (equating to 200 pulses). Helium was used as the carrier gas to efficiently transport aerosol to the ICP-MS. Zircon 91500 was used as the external standard to correct instrumental mass discrimination and elemental fractionation. Zircon GJ-1 and Plešovice were treated as quality control for geochronology. Lead concentrations in zircon were externally calibrated against NIST SRM 610 using Si as an internal standard, while Zr was used as an internal standard for other trace elements (Hu et al., 2011; Liu et al., 2010b). Raw data reduction was performed off-line by ICPMSDataCal software (Liu et al., 2010a, 2010b). Common Pb corrections were carried out using an Excel script (Andersen, 2002). Age calculations and concordia diagrams were made using Isoplot 4.0 (Ludwig, 2003).

3.2. In situ LA-ICP-MS cassiterite U-Pb dating

Sample WXL-17 was collected from the tin greisen in the eastern Hehuaping deposit, and samples IV-1 and IV-2 were obtained from the skarn orebody in the southwestern Hehuaping tin deposit (Fig. 2). Samples were crushed to 40–60 mesh, and cassiterite grains were separated using standard heavy liquid and magnetic separation techniques. Grains were then handpicked under a binocular microscope, mounted with an in-house external standard cassiterite (Lbiao) in an epoxy resin disc and then polished. Based on observations of internal textures under the microscope, inclusion-free cassiterite grains were selected for U–Pb analyses. *In situ* U–Pb dating on cassiterite was performed using a Neptune MC-ICP-MS (Thermo Fisher Scientific) coupled with an ESI 193 nm UP193FX ArF Excimer laser ablation system at the Tianjing Institute of Geology and Mineral Resources. The MC-ICP-MS instrument is equipped with nine Faraday cups, including one axial Faraday cup and eight off-axis Faraday cups, and four ion counters. The laser system is operated with a pulse of ~5 ns. Based on the reflected and transmitted light photomicrograph images, the laser was focused to produce an ablation pit with a beam diameter from 35 to 50 μm, using a laser pulse rate of 8–10 Hz with an energy density of 13–14 J/cm^2. To correct for the matrix effect, a cassiterite (Lbiao) with a U–Pb age of 158.2 ± 0.4 Ma (ID-TIMS)

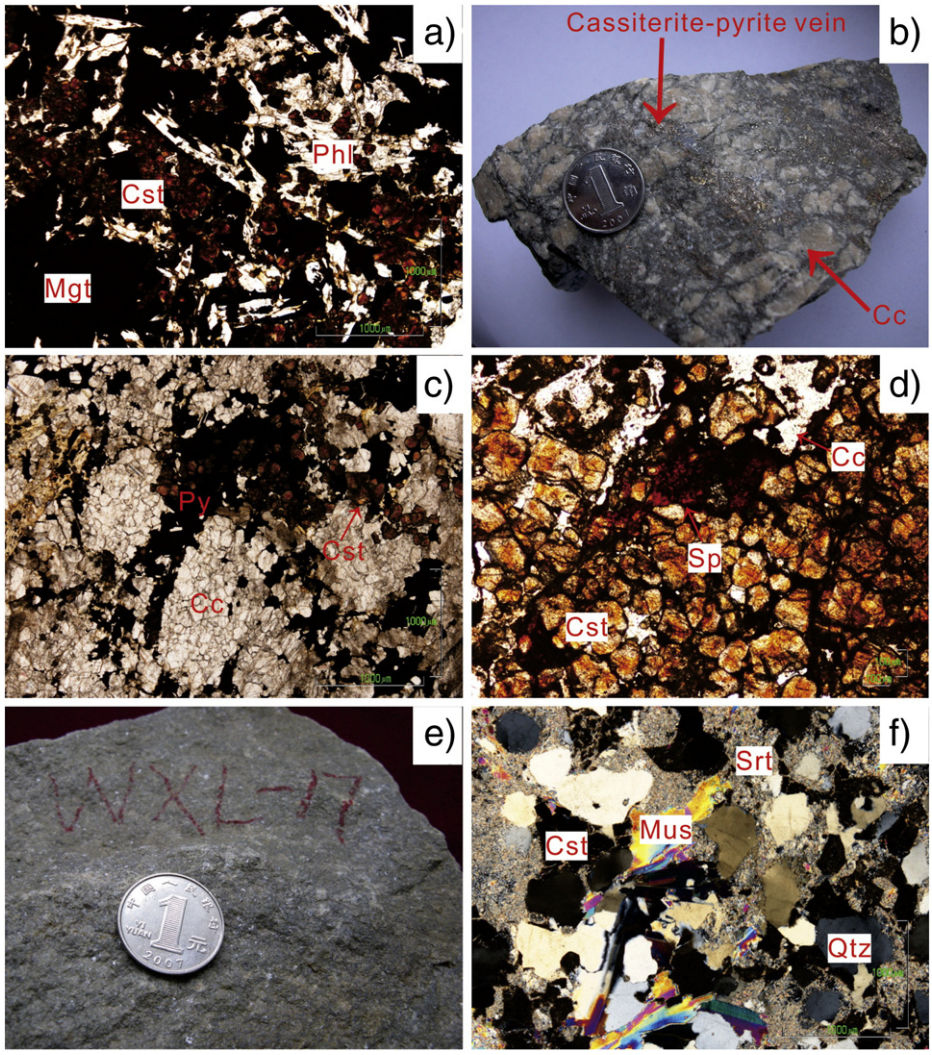

Fig. 8. Photographs and photomicrographs of tin ores from the Hehuaping tin deposit. (a) Photomicrograph of cassiterite–magnetite–phlogopite skarn from drill hole ZK4701 (crossed nicols). (b) Cassiterite–sulfide veins in marble. (c) Photomicrograph of cassiterite–sulfide veins crosscutting marble (crossed nicols). (d) Photomicrograph of cassiterite–sulfide vein in a granite porphyry dyke (crossed nicols). (e) Tin greisen. (f) Photomicrograph of cassiterite in tin greisen (crossed nicols). Abbreviations: Cst (cassiterite), Mus (muscovite), Srt (sericite), Cc (calcite), Qtz (quartz), Phl (Phlogopite), Mgt (magnetite), Py (pyrite), Sp (sphalerite).

was used as an in-house external standard during *in situ* LA-ICP-MS U–Pb analyses (Yuan et al., 2011). For each analysis of an unknown, one external standard measurement was also made. Each analysis incorporated a background acquisition of 20 s followed by 40 s sample data acquisition. Details of instrument parameters and conditions are the same as those described by Yuan et al. (2011). The $^{207}Pb/^{206}Pb$, $^{206}Pb/^{238}U$ and $^{207}Pb/^{235}U$ ratios were corrected using the cassiterite external standard, and calculated ages were determined using Isoplot 4.0.

3.3. Molybdenite Re–Os dating

Five molybdenite separates were obtained from tourmaline–quartz veins in the Yejiwo tungsten deposit; the molybdenite is associated with muscovite and scheelite. Eight molybdenite separates were collected from quartz–wolframite veins in the Shuiyuanshan tungsten deposit. The separates were handpicked under a binocular microscope, and then crushed to 200 meshes. Molybdenite Re–Os isotopic analyses were carried out in the Re–Os laboratory at the National Research Centre of Geoanalysis in Beijing, China. The detailed analytical method was described by Du et al. (2001, 2004) and Qu and Du (2003). Molybdenite separates were digested by HNO_3–HCl in a Carius tube (Shirey and Walker, 1995). The tube was then placed in a stainless steel jacket and heated for 10 hours at 230 °C. The Re was separated by solvent extraction and cation exchange resin chromatography. Re and Os concentrations were determined using a Thermo X-series ICP–MS. The mean value of the molybdenite standard GBW04435 (JDC) analyzed in this study was 141.1 ± 1.9 Ma, consistent with the published value of 139.6 ± 3.8 Ma (Du et al., 2004). Analytical blanks were 4.3 pg for Re and 0.09 pg for Os. ^{187}Re has a decay constant of $1.666 \pm 0.017 \times 10^{-11}y^{-1}$ (Smoliar et al., 1996). The Re–Os isochron age was calculated using the least-squares method of York (1969) and plotted using the Isoplot 4.0.

3.4. Muscovite ^{40}Ar–^{39}Ar dating

One muscovite separate (WXL-2) was collected from scheelite greisen in the Shuiyuanshan tungsten deposit. Muscovite is associated with quartz, scheelite and fluorite. The separates were washed repeatedly in an ultrasonic bath using deionized water and acetone. Aliquots of ~10 mg were wrapped in Al foil and stacked in quartz vials. After samples were stacked, the sealed quartz vials were put in a quartz canister, which was wrapped with cadmium foil (0.5 mm in thickness) for shielding slow neutrons and for preventing interface reactions during irradiation. Samples were irradiated for 30 hours in channel B4 of the Beijing 49-2 reactor at the Chinese Academy of Nuclear-Energy Sciences, Beijing, China. During irradiation, the vials were rotated at a speed of two cycles per minute to ensure uniformity of the irradiation. The muscovite standard

Table 3
In situ LA-ICP-MS U–Pb dating results for zircons from the granitic rocks in the Wangxianling area.

Sample spots	Th/ppm	U/ppm	Th/U	$^{207}Pb/^{206}Pb$	1σ	$^{207}Pb/^{235}U$	1σ	$^{206}Pb/^{238}U$	1σ	$^{208}Pb/^{232}Th$	1σ	$^{207}Pb/^{206}Pb$ Age (Ma)	1σ	$^{207}Pb/^{235}U$ Age (Ma)	1σ	$^{206}Pb/^{238}U$ Age (Ma)	1σ	$^{208}Pb/^{232}Th$ Age (Ma)	1σ
Wangxianling tourmaline two-mica (muscovite) granite																			
WXL10-5-01	150	424	0.35	0.10803	0.00267	4.66963	0.11731	0.31394	0.00491	0.04384	0.00434	1766	46	1762	21	1760	24	867	84
WXL10-5-02	1729	6838	0.25	0.11336	0.01182	0.49384	0.05048	0.03160	0.00065	0.00911	0.00035	1854	196	408	34	201	4	183	7
WXL10-5-03	1889	1442	1.31	0.07521	0.00236	0.37336	0.01171	0.03603	0.00064	0.00495	0.00046	1074	65	322	9	228	4	100	9
WXL10-5-04	929	820	1.13	0.10679	0.00198	3.97409	0.07812	0.26997	0.00378	0.05052	0.00442	1745	35	1629	16	1541	19	996	85
WXL10-5-05	2369	1094	2.16	0.05300	0.00155	0.25958	0.00754	0.03553	0.00054	0.00706	0.00082	329	68	234	6	225	3	142	16
WXL10-5-06	74	867	0.09	0.06119	0.00270	0.86963	0.03763	0.10323	0.00215	0.01920	0.00378	646	97	635	20	633	13	384	75
WXL10-5-07	1185	2843	0.42	0.07417	0.00115	0.50198	0.00824	0.04909	0.00062	0.02694	0.00241	1046	32	413	6	309	4	537	47
WXL10-5-08	75	270	0.28	0.06373	0.00139	1.06361	0.02330	0.12106	0.00164	0.03261	0.00380	733	47	736	11	737	9	649	74
WXL10-5-09	108	602	0.18	0.06781	0.00318	1.12354	0.05109	0.12017	0.00140	0.03659	0.00046	863	100	765	24	732	8	726	9
WXL10-5-10	0	92	0.00	0.05827	0.00240	0.69605	0.02777	0.08665	0.00147	0.00655	0.00097	540	92	536	17	536	9	132	19
WXL10-5-11	1366	12022	0.11	0.04694	0.00145	0.22795	0.00693	0.03522	0.00054	0.02086	0.00477	46	67	209	6	223	3	417	94
WXL10-5-12	882	2976	0.30	0.06994	0.00168	0.33653	0.00795	0.03492	0.00046	0.04212	0.01033	927	50	295	6	221	3	834	200
WXL10-5-13	478	98	4.90	0.37415	0.00654	17.0832	0.29473	0.33117	0.00403	0.13975	0.02325	3808	26	2940	17	1844	20	2644	412
WXL10-5-14	2211	481	4.60	0.05234	0.00233	0.25471	0.01107	0.03530	0.00063	0.00970	0.00224	300	104	230	9	224	4	195	45
WXL10-5-15	632	481	1.31	0.05388	0.00190	0.26059	0.00910	0.03509	0.00058	0.01174	0.00158	366	81	235	7	222	4	236	32
WXL10-5-16	4844	1234	3.93	0.05189	0.00121	0.25170	0.00604	0.03520	0.00052	0.00996	0.00122	281	55	228	5	223	3	200	24
WXL10-5-17	532	5101	0.10	0.05189	0.00086	0.25137	0.00411	0.03514	0.00040	0.01688	0.00220	281	39	228	3	223	2	338	44
WXL10-5-18	1225	763	1.61	0.08000	0.00234	0.53782	0.01586	0.04881	0.00084	0.01063	0.00135	1197	59	437	10	307	5	214	27
WXL10-5-19	341	7369	0.05	0.05909	0.00116	0.28825	0.00594	0.03539	0.00050	0.05200	0.00736	570	44	257	5	224	3	1025	141
WXL10-5-20	291	396	0.74	0.06705	0.00179	1.09203	0.02970	0.11824	0.00191	0.03263	0.00418	839	57	749	14	720	11	649	82
WXL10-5-21	120	164	0.73	0.08725	0.00362	2.82150	0.11203	0.23457	0.00445	0.06735	0.01709	1366	82	1361	30	1358	23	1317	324
WXL10-5-22	2477	17732	0.14	0.12788	0.00198	0.35354	0.00577	0.02005	0.00025	0.05437	0.00592	2069	28	307	4	128	2	1070	113
WXL10-5-23	150	787	0.19	0.05212	0.00210	0.25645	0.00985	0.03568	0.00057	0.01442	0.00459	291	94	232	8	226	4	289	91
WXL10-5-24	529	684	0.77	0.05072	0.00109	0.24574	0.00525	0.03514	0.00044	0.01117	0.00118	228	51	223	4	223	3	225	24
WXL10-5-25	244	228	1.07	0.07100	0.00241	1.56970	0.05206	0.16038	0.00265	0.04435	0.00857	957	71	958	21	959	15	877	166
WXL10-5-26	1352	533	2.54	0.07136	0.00201	1.59177	0.04406	0.16179	0.00239	0.03916	0.00631	968	59	967	17	967	13	776	123
WXL10-5-27	914	14065	0.06	0.05525	0.00105	0.18709	0.00376	0.02456	0.00034	0.01526	0.00199	422	43	174	3	156	2	306	40
WXL10-10-01	141	595	0.24	0.05090	0.00088	0.25408	0.00456	0.03621	0.00045	0.01072	0.00064	236	41	230	4	229	3	216	13
WXL10-10-02	5186	4790	1.08	0.04983	0.00085	0.19753	0.00368	0.02875	0.00040	0.00815	0.00063	187	41	183	3	183	3	164	13
WXL10-10-03	1705	1250	1.36	0.05259	0.00087	0.25876	0.00432	0.03570	0.00041	0.01075	0.00085	311	39	234	3	226	3	216	17
WXL10-10-04	804	1236	0.65	0.04605	0.00484	0.40589	0.04234	0.06393	0.00084	0.02057	0.00130		214	346	31	399	5	412	26
WXL10-10-05	506	9240	0.05	0.07396	0.00124	0.25280	0.00472	0.02479	0.00035	0.04238	0.00367	1040	35	229	4	158	2	839	71
WXL10-10-06	903	1882	0.48	0.06643	0.00108	0.64035	0.01147	0.06992	0.00097	0.02278	0.00176	820	35	503	7	436	6	455	35
WXL10-10-07	172	2799	0.06	0.05158	0.00097	0.25052	0.00467	0.03524	0.00042	0.01261	0.00143	267	44	227	4	223	3	253	29
WXL10-10-08	396	6784	0.06	0.04920	0.00145	0.19500	0.00516	0.02874	0.00037	0.00909	0.00014	158	70	181	4	183	2	183	3
WXL10-10-09	932	11387	0.08	0.04605	0.00165	0.05608	0.00184	0.00883	0.00013	0.00593	0.00215		75	55	2	57	1	119	43
WXL10-10-10	281	776	0.36	0.04605	0.00332	0.21802	0.01539	0.03434	0.00050	0.01135	0.00100		160	200	13	218	3	228	20
WXL10-10-11	410	18709	0.02	0.05803	0.00104	0.19669	0.00386	0.02459	0.00035	0.03850	0.00406	531	40	182	3	157	2	764	79
WXL10-10-12	869	1131	0.77	0.06246	0.00174	0.29314	0.00813	0.03404	0.00051	0.01262	0.00176	690	61	261	6	216	3	253	35
WXL10-10-13	1386	921	1.51	0.05403	0.00102	0.26209	0.00520	0.03518	0.00048	0.01110	0.00104	372	43	236	4	223	3	223	21
WXL10-10-14	1084	3052	0.36	0.06905	0.00137	0.33777	0.00690	0.03546	0.00048	0.02012	0.00248	900	42	295	5	225	3	403	49
WXL10-10-15	1125	2667	0.42	0.06978	0.00129	0.33537	0.00624	0.03486	0.00043	0.02657	0.00297	922	39	294	5	221	3	530	58
WXL10-10-16	880	3125	0.28	0.07174	0.00105	0.33143	0.00497	0.03351	0.00039	0.01965	0.00163	979	31	291	4	212	2	393	32
WXL10-10-17	267	310	0.86	0.08596	0.00256	0.28937	0.00828	0.02442	0.00035	0.01650	0.00171	1337	59	258	7	156	2	331	34
WXL10-10-18	43	299	0.14	0.04976	0.00360	0.24097	0.01697	0.03512	0.00059	0.01109	0.00082	184	165	219	14	223	4	223	16
WXL10-10-19	295	945	0.31	0.08328	0.00129	0.41159	0.00662	0.03584	0.00044	0.03106	0.00238	1276	31	350	5	227	3	618	47
WXL10-10-20	4531	35538	0.13	0.05580	0.00125	0.18958	0.00420	0.02464	0.00033	0.01629	0.00224	444	51	176	4	157	2	327	45
WXL10-10-21	5222	4875	1.07	0.08430	0.02188	0.23528	0.06066	0.02024	0.00061	0.00602	0.00014	1299	571	215	50	129	4	121	3
WXL10-10-22	176	17977	0.01	0.05086	0.00149	0.16920	0.00431	0.02413	0.00035	0.00760	0.00041	234	69	159	4	154	2	153	8
WXL10-10-23	781	10882	0.07	0.05181	0.00150	0.19452	0.00506	0.02723	0.00034	0.00856	0.00012	277	68	180	4	173	2	172	2
WXL10-10-24	334	2756	0.12	0.05757	0.00118	0.27116	0.00559	0.03416	0.00044	0.01692	0.00222	513	46	244	4	217	3	339	44
MJL07-01	210	297	0.71	0.07919	0.01326	1.92907	0.32049	0.17668	0.00371	0.05289	0.00102	1177	358	1091	111	1049	20	1042	20
MJL07-02	147	798	0.18	0.09038	0.00495	0.95854	0.05079	0.07692	0.00108	0.02270	0.00062	1434	107	683	26	478	6	454	12
MJL07-04	437	9903	0.04	0.05060	0.00119	0.16586	0.00401	0.02378	0.00041	0.00240	0.00012	223	56	156	3	152	3	48	2
MJL07-05	1617	1954	0.83	0.05052	0.00089	0.25849	0.00500	0.03712	0.00054	0.00417	0.00018	219	42	233	4	235	3	84	4
MJL07-06	562	6251	0.09	0.05069	0.00130	0.27163	0.00722	0.03890	0.00067	0.01076	0.00075	227	61	244	6	246	4	216	15
MJL07-07	1049	5340	0.20	0.06342	0.00123	0.31115	0.00629	0.03559	0.00049	0.02354	0.00219	722	42	275	5	225	3	470	43
MJL07-08	672	458	1.47	0.08763	0.00223	0.42934	0.01098	0.03553	0.00056	0.01084	0.00084	1374	50	363	8	225	3	218	17
MJL07-09	1781	2656	0.67	0.05849	0.00127	0.28916	0.00632	0.03586	0.00050	0.00989	0.00120	548	49	258	5	227	3	199	24
MJL07-10	344	8555	0.04	0.05522	0.00583	0.25362	0.02645	0.03331	0.00053	0.01039	0.00178	421	241	230	21	211	3	209	36
MJL07-11	654	854	0.77	0.05476	0.0025	0.51514	0.02306	0.06829	0.00157	0.00531	0.00045	402	105	422	15	426	9	107	9
MJL07-12	402	649	0.62	0.05075	0.00145	0.25191	0.00734	0.03600	0.00059	0.00474	0.00035	229	68	228	6	228	4	96	7
MJL07-13	317	1343	0.24	0.13704	0.00342	1.94373	0.04019	0.10287	0.00144	0.02910	0.00043	2190	44	1096	14	631	8	580	8
MJL07-14	287	304	0.94	0.06491	0.00120	1.13454	0.02139	0.12678	0.00164	0.04001	0.00336	771	40	770	10	769	9	793	65
MJL07-15	575	769	0.75	0.05462	0.00168	0.45799	0.01420	0.06083	0.00107	0.00765	0.00052	397	71	383	10	381	7	154	10
MJL07-16	385	5485	0.07	0.05124	0.00112	0.24638	0.00549	0.03489	0.00061	0.00625	0.00024	252	51	224	4	221	4	126	5
MJL07-17	5927	12956	0.46	0.04993	0.00084	0.20544	0.00388	0.02984	0.00045	0.00382	0.00019	192	40	190	3	190	3	77	4
MJL07-18	916	14981	0.06	0.05000	0.00088	0.21178	0.00409	0.03071	0.00049	0.00692	0.00025	195	42	195	3	195	3	139	5
MJL07-19	1024	2774	0.37	0.05433	0.00133	0.46561	0.01141	0.06220	0.00112	0.00111	0.00005	385	56	388	8	389	7	22	1
MJL07-20	585	973	0.60	0.05013	0.00118	0.24594	0.00598	0.03559	0.00054	0.00672	0.00045	201	56	223	5	225	3	135	9
MJL07-21	117	366	0.32	0.10778	0.00147	3.73538	0.05695	0.25138	0.00326	0.06970	0.00422	1762	26	1579	12	1446	17	1362	80

Table 3 (*continued*)

Sample spots	Th/ppm	U/ppm	Th/U	$^{207}Pb/^{206}Pb$	1σ	$^{207}Pb/^{235}U$	1σ	$^{206}Pb/^{238}U$	1σ	$^{208}Pb/^{232}Th$	1σ	$^{207}Pb/^{206}Pb$ Age (Ma)	1σ	$^{207}Pb/^{235}U$ Age (Ma)	1σ	$^{206}Pb/^{238}U$ Age (Ma)	1σ	$^{208}Pb/^{232}Th$ Age (Ma)	1σ
Wangxianling tourmaline muscovite granite																			
MJL07-22	2720	4165	0.65	0.05209	0.00103	0.25233	0.00520	0.03514	0.00048	0.00794	0.00077	289	46	228	4	223	3	160	15
MJL07-23	141	570	0.25	0.06231	0.00450	0.62122	0.04385	0.07231	0.00111	0.02223	0.00037	685	159	491	27	450	7	444	7
MJL07-24	1176	7735	0.15	0.08816	0.00410	0.28189	0.01241	0.02319	0.00035	0.00686	0.00020	1386	92	252	10	148	2	138	4
MJL07-25	328	6372	0.05	0.05696	0.00091	0.28017	0.00493	0.03567	0.00051	0.01137	0.00046	490	36	251	4	226	3	229	9
MJL07-26	344	1580	0.22	0.04605	0.00262	0.22029	0.01218	0.03470	0.00048	0.01311	0.00226		124	202	10	220	3	263	45
MJL07-27	81	3634	0.02	0.04998	0.00077	0.24736	0.00416	0.03590	0.00049	0.00986	0.00046	194	37	224	3	227	3	198	9
MJL07-28	605	6300	0.10	0.04862	0.01726	0.20121	0.07114	0.03001	0.00094	0.00951	0.01133	130	599	186	60	191	6	191	227
MJL07-29	790	3086	0.26	0.05297	0.00114	0.26163	0.00570	0.03582	0.00048	0.00842	0.00122	328	50	236	5	227	3	169	24
WXL1-00	362	4168	0.09	0.05035	0.00083	0.24494	0.00429	0.03529	0.00046	0.01281	0.00126	211	39	222	3	224	3	257	25
WXL1-01	84	86	0.98	0.16230	0.00317	10.7844	0.20119	0.47835	0.00521	0.13245	0.00291	2480	34	2505	17	2520	23	2514	52
WXL1-02	1491	7108	0.21	0.05188	0.00091	0.25875	0.00434	0.03575	0.00028	0.01446	0.00028	280	41	234	3	226	2	290	6
WXL1-03	170	2994	0.06	0.05047	0.00121	0.24800	0.0052	0.03564	0.00041	0.01124	0.00014	217	57	225	4	226	3	226	3
WXL1-04	397	4708	0.08	0.05020	0.00104	0.24658	0.00456	0.03563	0.00033	0.01124	0.00011	204	49	224	4	226	2	226	2
WXL1-05	149	210	0.71	0.11340	0.00175	5.04962	0.09189	0.31890	0.00393	0.08995	0.00172	1855	29	1828	15	1784	19	1741	32
WXL1-02	1491	7108	0.21	0.05188	0.00091	0.25875	0.00434	0.03575	0.00028	0.01446	0.00028	280	41	234	3	226	2	290	6
WXL1-03	170	2994	0.06	0.05047	0.00121	0.24800	0.00520	0.03564	0.00041	0.01124	0.00014	217	57	225	4	226	3	226	3
WXL1-04	397	4708	0.08	0.05020	0.00104	0.24658	0.00456	0.03563	0.00033	0.01124	0.00011	204	49	224	4	226	2	226	2
WXL1-05	149	210	0.71	0.11340	0.00175	5.04962	0.09189	0.31890	0.00393	0.08995	0.00172	1855	29	1828	15	1784	19	1741	32
WXL1-06	942	1911	0.49	0.05062	0.00093	0.24882	0.00438	0.03533	0.0003	0.01091	0.00020	224	44	226	4	224	2	219	4
WXL1-07	469	2854	0.16	0.05562	0.00098	0.25985	0.00438	0.03351	0.00026	0.01438	0.00029	437	40	235	4	212	2	289	6
WXL1-08	605	6188	0.10	0.05007	0.00090	0.23298	0.00427	0.03339	0.00036	0.01140	0.00027	198	42	213	4	212	2	229	5
WXL1-09	242	196	1.23	0.09259	0.00169	3.49733	0.06440	0.27125	0.00254	0.07638	0.00145	1479	35	1527	15	1547	13	1488	27
WXL1-10	83	1704	0.05	0.05404	0.00166	0.38072	0.01021	0.05110	0.00077	0.01598	0.00027	373	71	328	8	321	5	320	5
WXL1-11	183	4237	0.04	0.05350	0.00090	0.26627	0.00549	0.03561	0.00044	0.02111	0.00063	350	39	240	4	226	3	422	12
WXL1-12	78	2141	0.04	0.05082	0.00098	0.25405	0.00477	0.03602	0.00030	0.01433	0.00064	233	46	230	4	228	2	288	13
WXL1-13	228	483	0.47	0.28557	0.00648	16.4015	0.31676	0.41655	0.00498	0.10991	0.00139	3394	36	2901	18	2245	23	2108	25
WXL1-14	371	477	0.78	0.15944	0.00226	9.78384	0.14032	0.44067	0.00297	0.12090	0.00192	2450	25	2415	13	2354	13	2307	35
WXL1-15	113	3333	0.03	0.05011	0.00111	0.24181	0.00503	0.03500	0.00027	0.01104	0.00016	200	53	220	4	222	2	222	3
WXL1-16	114	274	0.42	0.10473	0.00209	4.76432	0.09443	0.32826	0.00311	0.09433	0.00206	1710	38	1779	17	1830	15	1822	38
WXL1-17	78	951	0.08	0.06875	0.00126	1.44098	0.02779	0.15085	0.00158	0.04331	0.00107	891	39	906	12	906	9	857	21
WXL1-18	159	2837	0.06	0.05168	0.00112	0.23017	0.00461	0.03230	0.00027	0.01016	0.00010	271	51	210	4	205	2	204	2
WXL1-19	169	964	0.17	0.10923	0.00245	2.00381	0.03924	0.13305	0.00146	0.03850	0.00049	1787	42	1117	13	805	8	764	10
WXL1-20	447	597	0.75	0.06835	0.00112	1.42231	0.02332	0.14965	0.00132	0.04257	0.00071	879	35	898	10	899	7	843	14
WXL1-21	57	1415	0.04	0.05765	0.00109	0.66650	0.01312	0.08279	0.00080	0.02696	0.00098	516	42	519	8	513	5	538	19
WXL1-22	196	4804	0.04	0.04988	0.00086	0.25012	0.00428	0.03596	0.00032	0.01228	0.00041	189	41	227	3	228	2	247	8
WXL1-23	234	382	0.61	0.05928	0.00139	0.84008	0.01926	0.10201	0.00107	0.03032	0.00065	577	52	619	11	626	6	604	13
WXL1-24	159	171	0.93	0.07149	0.00147	1.66377	0.03282	0.16680	0.00168	0.04758	0.00096	971	43	995	13	994	9	939	18
WXL1-25	267	2631	0.10	0.05092	0.00100	0.25457	0.0053	0.03576	0.00047	0.01102	0.00031	237	46	230	4	226	3	221	6
WXL1-26	210	237	0.88	0.06198	0.00174	0.98598	0.02633	0.11432	0.00123	0.03593	0.00081	674	62	697	13	698	7	714	16
Hehuaping biotite granite (Drill hole ZK4701)																			
HHPD42-1	547	1581	0.35	0.04935	0.00026	0.16839	0.00240	0.02474	0.00034	0.00169	0.00014	165	13	158	2	158	2	34	3
HHPD42-2	194	395	0.49	0.13314	0.01520	0.82653	0.14805	0.03073	0.0018	0.00884	0.00162	2140	237	612	82	195	11	178	32
HHPD42-3	224	461	0.49	0.05756	0.00063	0.20821	0.00376	0.02632	0.00047	0.00206	0.00018	513	25	192	3	167	3	41	4
HHPD42-4	503	3187	0.16	0.05020	0.00176	0.17160	0.00589	0.02472	0.00034	0.00781	0.00023	204	83	161	5	157	2	157	5
HHPD42-5	163	383	0.43	0.04946	0.00149	0.17162	0.00455	0.02517	0.00032	0.00848	0.00024	170	72	161	4	160	2	171	5
HHPD42-6	498	1778	0.28	0.06106	0.00211	0.21754	0.00876	0.02496	0.00033	0.00981	0.00033	641	76	200	7	159	2	197	7
HHPD42-7	146	406	0.36	0.05401	0.00190	0.18777	0.00610	0.02498	0.00036	0.00885	0.00026	371	81	175	5	159	2	178	5
HHPD42-8	26	341	0.07	0.07385	0.00046	1.51780	0.01349	0.14897	0.00113	0.01355	0.00201	1037	13	938	5	895	6	272	40
HHPD42-9	341	723	0.47	0.04831	0.00193	0.16313	0.00613	0.02449	0.00034	0.00776	0.00013	115	91	153	5	156	2	156	3
HHPD42-10	151	431	0.35	0.04852	0.00100	0.16838	0.00334	0.02484	0.00026	0.00843	0.00020	125	50	158	3	158	2	170	4
HHPD42-11	196	601	0.33	0.05779	0.00148	0.19990	0.00538	0.02451	0.00026	0.01105	0.00034	522	57	185	5	156	2	222	7
HHPD42-12	401	1041	0.38	0.04985	0.00143	0.17114	0.00483	0.02443	0.00030	0.00882	0.00023	188	68	160	4	156	2	178	5
HHPD42-13	407	1329	0.31	0.04970	0.00112	0.17129	0.00372	0.02451	0.00025	0.00914	0.00021	181	54	161	3	156	2	184	4
HHPD42-14	645	1559	0.41	0.05127	0.00121	0.17672	0.00430	0.02451	0.00028	0.00861	0.00020	253	56	165	4	156	2	173	4
HHPD42-15	158	288	0.55	0.04816	0.00121	0.16520	0.00393	0.02463	0.00033	0.00819	0.00019	107	60	155	3	157	2	165	4
HHPD42-16	159	687	0.23	0.05151	0.00106	0.17717	0.00404	0.02442	0.00027	0.00892	0.00020	264	48	166	3	156	2	179	4
HHPD42-17	721	4122	0.17	0.04662	0.00234	0.15664	0.00761	0.02437	0.00032	0.00776	0.00026	30	109	148	7	155	2	156	5
HHPD42-18	153	429	0.36	0.04967	0.00116	0.17095	0.00392	0.02466	0.00026	0.00835	0.00019	180	56	160	3	157	2	168	4
HHPD42-19	147	377	0.39	0.05319	0.00052	0.19691	0.00262	0.02684	0.00027	0.00269	0.00029	337	23	183	2	171	2	54	6
HHPD42-20	443	1241	0.36	0.04965	0.00029	0.16849	0.0023	0.02458	0.00028	0.00195	0.00017	178	14	158	2	157	2	39	4
HHPD42-22	104	216	0.48	0.06320	0.00161	0.21554	0.00606	0.02467	0.00029	0.00354	0.00044	715	55	198	5	157	2	72	9
HHPD42-23	309	619	0.50	0.04779	0.00038	0.16295	0.00320	0.02472	0.00046	0.00191	0.00019	89	19	153	3	157	3	39	4
HHPD42-24	1465	8061	0.18	0.05125	0.00024	0.17406	0.00269	0.02462	0.00037	0.00187	0.00013	252	11	163	2	157	2	38	3
HHPD42-25	851	6231	0.14	0.05293	0.00026	0.17897	0.00297	0.02452	0.00041	0.00207	0.00016	326	12	167	3	156	3	42	3
HHPD42-26	514	2403	0.21	0.04870	0.00020	0.16641	0.00279	0.02478	0.00041	0.00187	0.00015	133	10	156	2	158	3	38	3
HHPD42-27	161	448	0.36	0.04995	0.00040	0.17021	0.00249	0.02471	0.00032	0.00274	0.00030	193	19	160	2	157	2	55	6
HHPD42-28	163	454	0.36	0.04866	0.00053	0.16442	0.00226	0.02455	0.00029	0.00255	0.00029	131	26	155	2	156	2	51	6
HHPD42-30	152	345	0.44	0.05401	0.00091	0.18538	0.00524	0.02468	0.00038	0.00225	0.00027	371	39	173	4	157	2	45	5
HHPD42-31	656	2587	0.25	0.04917	0.00023	0.16912	0.00206	0.02495	0.00031	0.00203	0.00019	156	11	159	2	159	2	41	4
HHPD42-33	359	2588	0.14	0.04914	0.00032	0.20447	0.00415	0.03007	0.00051	0.00237	0.00026	155	16	189	3	191	3	48	5

(*continued on next page*)

Table 3 (*continued*)

Sample spots	Th/ppm	U/ppm	Th/U	$^{207}Pb/^{206}Pb$	1σ	$^{207}Pb/^{235}U$	1σ	$^{206}Pb/^{238}U$	1σ	$^{208}Pb/^{232}Th$	1σ	$^{207}Pb/^{206}Pb$ Age (Ma)	1σ	$^{207}Pb/^{235}U$ Age (Ma)	1σ	$^{206}Pb/^{238}U$ Age (Ma)	1σ	$^{208}Pb/^{232}Th$ Age (Ma)	1σ
Hehuaping biotite granite (Drill hole ZK6302)																			
6302-38-01	218	244	0.89	0.04903	0.00191	0.19650	0.00765	0.02906	0.00045	0.00627	0.00038	149	91	182	6	185	3	126	8
6302-38-02	31	218	0.14	0.06035	0.00225	0.18157	0.00662	0.02182	0.00030	0.01376	0.00130	616	82	169	6	139	2	276	26
6302-38-03	1877	11158	0.17	0.05031	0.00067	0.11651	0.00175	0.01680	0.00022	0.00521	0.00031	209	32	112	2	107	1	105	6
6302-38-04	796	2422	0.33	0.05019	0.00388	0.17729	0.01295	0.02576	0.00068	0.00517	0.00174	204	176	166	11	164	4	104	35
6302-38-05	781	2099	0.37	0.04976	0.00075	0.16809	0.00261	0.02450	0.00029	0.00745	0.00055	184	36	158	2	156	2	150	11
6302-38-06	179	235	0.77	0.05493	0.00203	0.18612	0.00685	0.02457	0.00036	0.00756	0.00053	409	85	173	6	156	2	152	11
6302-38-07	347	878	0.40	0.04815	0.00352	0.15979	0.01148	0.02407	0.00032	0.00763	0.00031	107	164	151	10	153	2	154	6
6302-38-08	325	786	0.41	0.06191	0.00139	0.20814	0.00481	0.02438	0.00035	0.00792	0.00063	671	49	192	4	155	2	159	13
6302-38-09	180	382	0.47	0.05230	0.00121	0.17462	0.00412	0.02422	0.00031	0.00753	0.00052	299	54	163	4	154	2	152	10
6302-38-10	147	177	0.83	0.04920	0.00316	0.14851	0.00933	0.02190	0.00039	0.00713	0.00101	157	146	141	8	140	2	144	20
6302-38-11	170	153	1.11	0.14795	0.00378	8.86337	0.23727	0.43369	0.00700	0.08248	0.01236	2322	45	2324	24	2322	31	1602	231
6302-38-12	1330	2908	0.46	0.05615	0.00087	0.18956	0.00323	0.02448	0.00032	0.00871	0.00073	458	35	176	3	156	2	175	15
6302-38-13	5452	26991	0.20	0.04605	0.00186	0.08317	0.00320	0.01310	0.00016	0.00440	0.00041		85	81	3	84	1	89	8
6302-38-14	114	210	0.55	0.05582	0.00238	0.18844	0.00798	0.02448	0.00039	0.01180	0.00117	445	97	175	7	156	2	237	23
6302-38-15	953	2233	0.43	0.05425	0.00096	0.18226	0.00344	0.02437	0.00033	0.00750	0.00058	381	41	170	3	155	2	151	12
6302-38-17	265	628	0.42	0.07069	0.00122	1.33989	0.02505	0.13749	0.00194	0.04047	0.00356	948	36	863	11	830	11	802	69
6302-38-18	417	679	0.61	0.04928	0.00161	0.17609	0.00578	0.02592	0.00042	0.00714	0.00071	161	78	165	5	165	3	144	14
6302-38-19	3248	49812	0.07	0.06269	0.00091	0.14822	0.00237	0.01714	0.00023	0.05760	0.00510	698	32	140	2	110	1	1132	97
6302-38-20	223	1625	0.14	0.05037	0.00287	0.17033	0.00941	0.02449	0.00051	0.01164	0.00362	212	132	160	8	156	3	234	72
6302-38-21	1037	949	1.09	0.05074	0.00163	0.15409	0.00488	0.02202	0.00033	0.00763	0.00100	229	76	146	4	140	2	154	20
6302-38-22	305	861	0.35	0.05639	0.00118	0.50537	0.01096	0.06501	0.00092	0.02172	0.00260	468	47	415	7	406	6	434	51
6302-38-24	2802	6853	0.41	0.04922	0.00100	0.14293	0.00309	0.02107	0.00032	0.00569	0.00062	158	49	136	3	134	2	115	12
6302-38-23	3182	33905	0.09	0.04891	0.00098	0.08289	0.00176	0.01230	0.00018	0.00537	0.00076	144	48	81	2	79	1	108	15
6302-38-25	247	397	0.62	0.04886	0.00262	0.16552	0.00872	0.02458	0.00049	0.00494	0.00062	141	122	156	8	157	3	100	12
6302-38-26	326	491	0.66	0.07085	0.00451	0.23910	0.01464	0.02448	0.00062	0.00801	0.00160	953	134	218	12	156	4	161	32
6302-38-27	1419	1684	0.84	0.05351	0.00121	0.18007	0.00419	0.02441	0.00036	0.00741	0.00096	350	52	168	4	155	2	149	19
Granite porphyry dyke																			
HHPP45-1	151	317	0.48	0.04891	0.00044	0.16287	0.00204	0.02418	0.00027	0.00207	0.00025	144	22	153	2	154	2	42	5
HHPP45-2	239	477	0.50	0.05036	0.00054	0.16837	0.00207	0.02430	0.00026	0.00216	0.00021	212	25	158	2	155	2	44	4
HHPP45-3	176	195	0.90	0.04968	0.00079	0.16557	0.00278	0.02424	0.00026	0.00216	0.00024	180	38	156	2	154	2	44	5
HHPP45-4	279	553	0.51	0.04864	0.00036	0.16289	0.00188	0.02430	0.00025	0.00188	0.00017	131	18	153	2	155	2	38	3
HHPP45-5	163	357	0.46	0.04833	0.00047	0.16134	0.00248	0.02421	0.00028	0.00212	0.00024	115	24	152	2	154	2	43	5
HHPP45-6	440	1006	0.44	0.05402	0.00046	0.18082	0.00274	0.02426	0.00029	0.00216	0.00016	372	20	169	2	155	2	44	3
HHPP45-7	111	258	0.43	0.04974	0.00053	0.16625	0.00247	0.02431	0.00033	0.00291	0.00032	183	25	156	2	155	2	59	7
HHPP45-8	331	373	0.89	0.05912	0.00026	0.80120	0.01068	0.09829	0.00127	0.00807	0.00051	571	10	598	6	604	7	162	10
HHPP45-9	53	187	0.28	0.05384	0.00098	0.18004	0.00338	0.02438	0.00032	0.00622	0.00068	364	42	168	3	155	2	125	14
HHPP45-10	157	375	0.42	0.04855	0.00048	0.16372	0.00267	0.02447	0.00033	0.00241	0.00025	126	24	154	2	156	2	49	5
HHPP45-11	164	409	0.40	0.04804	0.00054	0.16099	0.00239	0.02434	0.00031	0.00244	0.00028	101	27	152	2	155	2	49	6
HHPP45-12	123	281	0.44	0.05439	0.00070	0.18112	0.00253	0.02426	0.00029	0.00303	0.00030	387	30	169	2	155	2	61	6
HHPP45-13	115	288	0.40	0.05267	0.00089	0.17604	0.00282	0.02436	0.00026	0.00316	0.00032	315	40	165	2	155	2	64	6
HHPP45-14	450	566	0.79	0.05039	0.00039	0.16823	0.00192	0.02427	0.00027	0.00177	0.00013	213	18	158	2	155	2	36	3
HHPP45-15	155	357	0.43	0.05352	0.00084	0.17892	0.00283	0.02428	0.00017	0.00259	0.00026	351	36	167	2	155	1	52	5
HHPP45-16	126	258	0.49	0.05113	0.00073	0.16980	0.00242	0.02419	0.00026	0.00270	0.00027	247	34	159	2	154	2	55	5
HHPP45-17	286	633	0.45	0.05098	0.00040	0.17116	0.00159	0.02436	0.00017	0.00179	0.00016	240	19	160	1	155	1	36	3
HHPP45-18	376	852	0.44	0.04997	0.00046	0.16671	0.00187	0.02427	0.00028	0.00198	0.00016	194	22	157	2	155	2	40	3
HHPP45-19	121	251	0.48	0.05970	0.00089	0.19953	0.00278	0.02431	0.00019	0.00308	0.00031	593	33	185	2	155	1	62	6
HHPP45-20	166	387	0.43	0.05227	0.00058	0.17405	0.00181	0.02422	0.00021	0.00196	0.00021	297	26	163	2	154	1	40	4
HHPP45-21	343	1270	0.27	0.04891	0.00030	0.16458	0.00135	0.02443	0.00020	0.00174	0.00016	143	14	155	1	156	1	35	3
HHPP45-22	103	220	0.47	0.05445	0.00085	0.18154	0.00274	0.02427	0.00022	0.00260	0.00033	390	36	169	2	155	1	52	7
HHPP45-23	388	923	0.42	0.05087	0.00025	0.17034	0.00133	0.02429	0.00018	0.00172	0.00014	235	11	160	1	155	1	35	3
HHPP45-24	107	218	0.49	0.05448	0.00094	0.18150	0.00232	0.02432	0.00019	0.00305	0.00029	391	40	169	2	155	1	62	6
HHPP45-25	148	342	0.43	0.04992	0.00053	0.16710	0.00167	0.02433	0.00017	0.00225	0.00020	191	25	157	1	155	1	45	4
HHPP45-26	299	538	0.56	0.05600	0.00044	0.18723	0.00140	0.02428	0.00016	0.00190	0.00014	452	18	174	1	155	1	38	3
HHPP45-27	146	423	0.35	0.15976	0.01117	0.74602	0.06599	0.02990	0.00077	0.00747	0.00079	2453	122	566	38	190	5	150	16
HHPP45-28	71	150	0.47	0.06968	0.00175	0.23252	0.00717	0.02403	0.00024	0.00368	0.00034	919	53	212	6	153	2	74	7
HHPP45-29	147	311	0.47	0.05095	0.00055	0.16980	0.00178	0.02420	0.00016	0.00236	0.00022	238	26	159	2	154	1	48	4
HHPP45-30	145	312	0.47	0.05040	0.00050	0.16877	0.00191	0.02428	0.00016	0.00179	0.00019	213	23	158	2	154.7	1	36	4
HHPP45-31	203	495	0.41	0.04822	0.00030	0.16157	0.00125	0.02431	0.00016	0.00196	0.00016	110	15	152	1	155	1	40	3
DGL106-01	5022	15135	0.33	0.04870	0.00141	0.12821	0.00353	0.01909	0.00017	0.00605	0.00006	134	69	122	3	122	1	122	1
DGL106-02	2128	5127	0.42	0.06533	0.00183	0.22833	0.00609	0.02501	0.00022	0.01127	0.00037	785	60	209	5	159	1	227	7
DGL106-03	822	2709	0.30	0.05112	0.00096	0.17341	0.00315	0.02426	0.00022	0.00870	0.00019	246	44	162	3	155	1	175	4
DGL106-04	1063	1998	0.53	0.05031	0.00104	0.17623	0.00387	0.02496	0.00026	0.00825	0.00018	209	49	165	3	159	2	166	4
DGL106-05	305	608	0.50	0.05020	0.00176	0.17160	0.00589	0.02472	0.00034	0.00781	0.00023	204	83	161	5	157	2	157	5
DGL106-06	369	883	0.42	0.04946	0.00149	0.17162	0.00455	0.02517	0.00032	0.00848	0.00024	170	72	161	4	160	2	171	5
DGL106-07	823	1803	0.46	0.06106	0.00211	0.21754	0.00876	0.02496	0.00033	0.00981	0.00033	641	76	200	7	159	2	197	7
DGL106-08	434	990	0.44	0.05401	0.00190	0.18777	0.00610	0.02498	0.00036	0.00885	0.00026	371	81	175	5	159	2	178	5
DGL106-09	196	463	0.42	0.04862	0.00238	0.16709	0.00784	0.02493	0.00035	0.00790	0.00017	129	112	157	7	159	2	159	3
DGL106-10	17437	32266	0.54	0.04918	0.00088	0.11167	0.00185	0.01618	0.00014	0.00521	0.00010	156	43	107	2	104	1	105	2
DGL106-11	563	1331	0.42	0.04831	0.00193	0.16313	0.00613	0.02449	0.00034	0.00776	0.00013	115	91	153	5	156	2	156	3
DGL106-12	789	1676	0.47	0.04852	0.00100	0.16838	0.00334	0.02484	0.00026	0.00843	0.00020	125	50	158	3	158	2	170	4
DGL106-13	324	885	0.37	0.04903	0.00151	0.17004	0.00532	0.02473	0.00038	0.00809	0.00026	149	74	159	5	158	2	163	5
DGL106-14	712	1671	0.43	0.04760	0.00106	0.16358	0.00350	0.02454	0.00026	0.00824	0.00018	80	52	154	3	156	2	166	4

Table 3 (*continued*)

Sample spots	Th/ppm	U/ppm	Th/U	$^{207}Pb/^{206}Pb$	1σ	$^{207}Pb/^{235}U$	1σ	$^{206}Pb/^{238}U$	1σ	$^{208}Pb/^{232}Th$	1σ	$^{207}Pb/^{206}Pb$ Age (Ma)	1σ	$^{207}Pb/^{235}U$ Age (Ma)	1σ	$^{206}Pb/^{238}U$ Age (Ma)	1σ	$^{208}Pb/^{232}Th$ Age (Ma)	1σ
Granite porphyry dyke																			
DGL106-15	514	1350	0.38	0.05071	0.00121	0.17828	0.00429	0.02513	0.00028	0.00847	0.00021	228	56	167	4	160	2	170	4
DGL106-16	1010	3912	0.26	0.05779	0.00148	0.19990	0.00538	0.02451	0.00026	0.01105	0.00034	522	57	185	5	156	2	222	7
DGL106-17	307	982	0.31	0.08013	0.00172	0.53433	0.01127	0.04740	0.00054	0.01088	0.00028	1200	43	435	7	299	3	219	6
DGL106-18	513	1232	0.42	0.04985	0.00143	0.17114	0.00483	0.02443	0.00030	0.00882	0.00023	188	68	160	4	156	2	178	5
DGL106-19	864	2590	0.33	0.04970	0.00112	0.17129	0.00372	0.02451	0.00025	0.00914	0.00021	181	54	161	3	156	2	184	4
DGL106-20	671	1397	0.48	0.05127	0.00121	0.17672	0.00430	0.02451	0.00028	0.00861	0.00020	253	56	165	4	156	2	173	4
DGL106-21	420	942	0.45	0.04816	0.00121	0.16520	0.00393	0.02463	0.00033	0.00819	0.00019	107	60	155	3	157	2	165	4
DGL106-22	832	2044	0.41	0.05151	0.00106	0.17717	0.00404	0.02442	0.00027	0.00892	0.00020	264	48	166	3	156	2	179	4
DGL106-23	362	1098	0.33	0.05153	0.00188	0.15991	0.00539	0.02232	0.00037	0.00929	0.00033	265	86	151	5	142	2	187	7
DGL106-24	853	2169	0.39	0.04662	0.00234	0.15664	0.00761	0.02437	0.00032	0.00776	0.00026	30	109	148	7	155	2	156	5
DGL106-25	800	2657	0.30	0.04967	0.00116	0.17095	0.00392	0.02466	0.00026	0.00835	0.00019	180	56	160	3	157	2	168	4

Bern4M (18.74 ± 0.20 Ma; Hall et al., 1984) was used to monitor the neutron flux. $^{40}Ar/^{39}Ar$ stepwise heating analyses were performed at the State Key Laboratory of Lithospheric Evolution, Institute of Geology and Geophysics, Chinese Academy of Sciences, Beijing, China, using a GV MM5400 mass spectrometer equipped with a Faraday cup and an ion counter for Ar isotopic measurement. The irradiated samples were loaded into a Christmas-tree-type sample holder and degassed at 200–250 °C for ~72 hours in a high vacuum system. The samples were analyzed in 13 temperature steps from 750 °C to total fusion at 1260 °C. Step-heating analysis was carried out in a double-vacuum resistance furnace. Samples were heated at each temperature step for 10 minutes, and the extracted gasses were purified by two SAES Zr-Al getters (NP10). K_2SO_4 and CaF_2 crystals were analyzed to calculate Ca and K correction factors: $[^{36}Ar/^{37}Ar]_{Ca} = 2.609 \times 10^{-4} \pm 1.418 \times 10^{-5}$; $[^{39}Ar/^{37}Ar]_{Ca} = 7.236 \times 10^{-4} \pm 2.814 \times 10^{-5}$; $[^{40}Ar/^{39}Ar]_{K} = 2.648 \times 10^{-2} \pm 2.254 \times 10^{-5}$. The decay constant used for age calculations was $\lambda = 5.543 \times 10^{-10} a^{-1}$ (Steiger and Jäger, 1977). Data-processing was performed using ArArCALC 2.4 software (Koppers, 2002). The $^{40}Ar/^{36}Ar$ vs. $^{39}Ar/^{36}Ar$ isochron diagram was constructed using Isoplot 4.0.

4. Results

4.1. Zircon U–Pb ages

The LA-ICP-MS analytical data are summarized in Table 3. Error on individual analysis is reported at the 1σ level, and the weighted mean $^{206}Pb/^{238}U$ ages are quoted at the 95% confidence level. For zircon younger than 1000 Ma, the weighted mean $^{206}Pb/^{238}U$ age is used for the assessment of its age, whereas the $^{207}Pb/^{206}U$ age is used for zircon with ages greater than 1000 Ma.

4.1.1. Wangxianling pluton

Twenty-seven spots of one sample (WXL10-5) from the Wangxianling central phase were selected for *in situ* U-Pb dating. As shown by the CL images, most zircon grains have bright inherited cores and black to bright rims (Fig. 9a). Three black rims have high U contents (6800–17700 ppm) and relatively low Th/U ratios (0.06–0.25). They yield younger $^{206}Pb/^{238}U$ ages from 128 to 201 Ma as a result of Pb loss, and therefore should be rejected. Seven inherited grains and six cores with variable U contents (92–2840 ppm) and Th/U ratios (0.18–4.9) yield U–Pb ages from 536 to 3808 Ma. The remaining 11 spots for magmatic rims and grains have variable U contents (480–12000 ppm) and Th/U ratios (0.1–4.6), and yield a weighted mean age of 223.5 ± 1.8 Ma (MSWD = 0.29) (Fig. 10a). This age represents the crystallization age of the Wangxianling central phase.

Zircons of three samples (WXL10-10, MJL07 and WXL-1) from the Wangxianling marginal phase show similar rim–core textures to zircons of the central phase (Fig. 9b–d). Twenty-four spots were measured for sample WXL10-10. Eleven black zircon grains and rims have cracks and mineral inclusions, high U concentrations ranging from 3130 to 35500 ppm, and variable Th/U ratios (0.06–1.08). Their younger $^{206}Pb/^{238}U$ ages from 56.7 to 212 Ma are as a result of Pb loss, and were therefore not used in age calculations. Two inherited cores with U contents of 1880 ppm and 1240 ppm had corresponding $^{206}Pb/^{238}U$ ages of 399 Ma and 436 Ma. One zircon grain (WXL10-10-17) has low Th and U contents (267 ppm and 310 ppm, respectively) but is discordant and has a younger age. Concentrations of U and Th for 11 magmatic grains range from 43 to 1710 ppm and 299 to 3050 ppm, respectively, with corresponding Th/U ratios of 0.06–1.51. They yield a weighted mean age of 222.5 ± 2.9 Ma (MSWD = 2.0), which is interpreted as the crystallization age of the sample (Fig. 10b). Twenty-nine analytical spots were obtained for sample MJL07 (Fig. 10c). Four zircon grains and three zircon rims have cracks and mineral inclusions with high U contents (6300–14900 ppm), low Th/U ratios (0.06–0.47) and younger $^{206}Pb/^{238}U$ ages (148–211 Ma). These zircons are interpreted as Pb loss affected grains, and therefore should be rejected. Nine zircon grains have bright and clear inherited cores with U concentrations of 297–2770 ppm and Th/U ratios of 0.18–0.94, and yield U-Pb ages ranging from 389 to 1762 Ma. Spots MJL07-5 and MJL07-6 for two zircon grains with narrow rims and large cores have concordant ages of 235 Ma and 246 Ma, which are likely to represent the mixing ages of the magmatic rims with inherited cores. The remaining 11 zircon grains have U contents and Th/U ratios ranging from 970 to 6400 ppm and from 0.02 to 1.47, respectively. Their weighted mean $^{206}Pb/^{238}U$ age is 224.9 ± 1.7 Ma (MSWD = 2.5) representing the crystallization age of the sample. A total of 27 spots were analyzed on 14 grains from sample WXL-1 (Fig. 10d). The zircon grains from this sample contain many inclusions and cracks. Ten inherited cores and four grains with Th and U contents ranging from 78 to 447 ppm and 86 to 960 ppm, respectively, have a large spread in ages from 321 to 2480 Ma. Three rims with cracks have U contents ranging from 2840 to 6190 ppm. They yield younger ages from 206 to 212 Ma as a result of Pb loss, and therefore are rejected from the analyses. Ten magmatic rims with U contents ranging from 2140 to 7100 ppm yield a weighted mean $^{206}Pb/^{238}U$ age of 225.6 ± 1.4 Ma (MSWD = 0.8) representing the crystallization age of the sample.

To summarize, the zircon U–Pb dating of the four granite samples indicates that the Wangxianling pluton crystallized at ~224 Ma.

4.1.2. Hehuaping pluton

Zircons from two biotite granite samples (HHPD42 and 6302-38) are 30–100 μm in length and 30–50 μm in width. Most grains are colorless and have bright CL (Fig. 9e, f). A handful of grains are yellow or brown to black, with tiny inclusions and many cracks, and are characterized by dark CL and blurry oscillatory zoning. Thirty grains were analyzed for sample HHPD42 (Fig. 10e). Three grains have discordant ages and are rejected. Two inherited zircon grains have $^{206}Pb/^{238}U$ ages

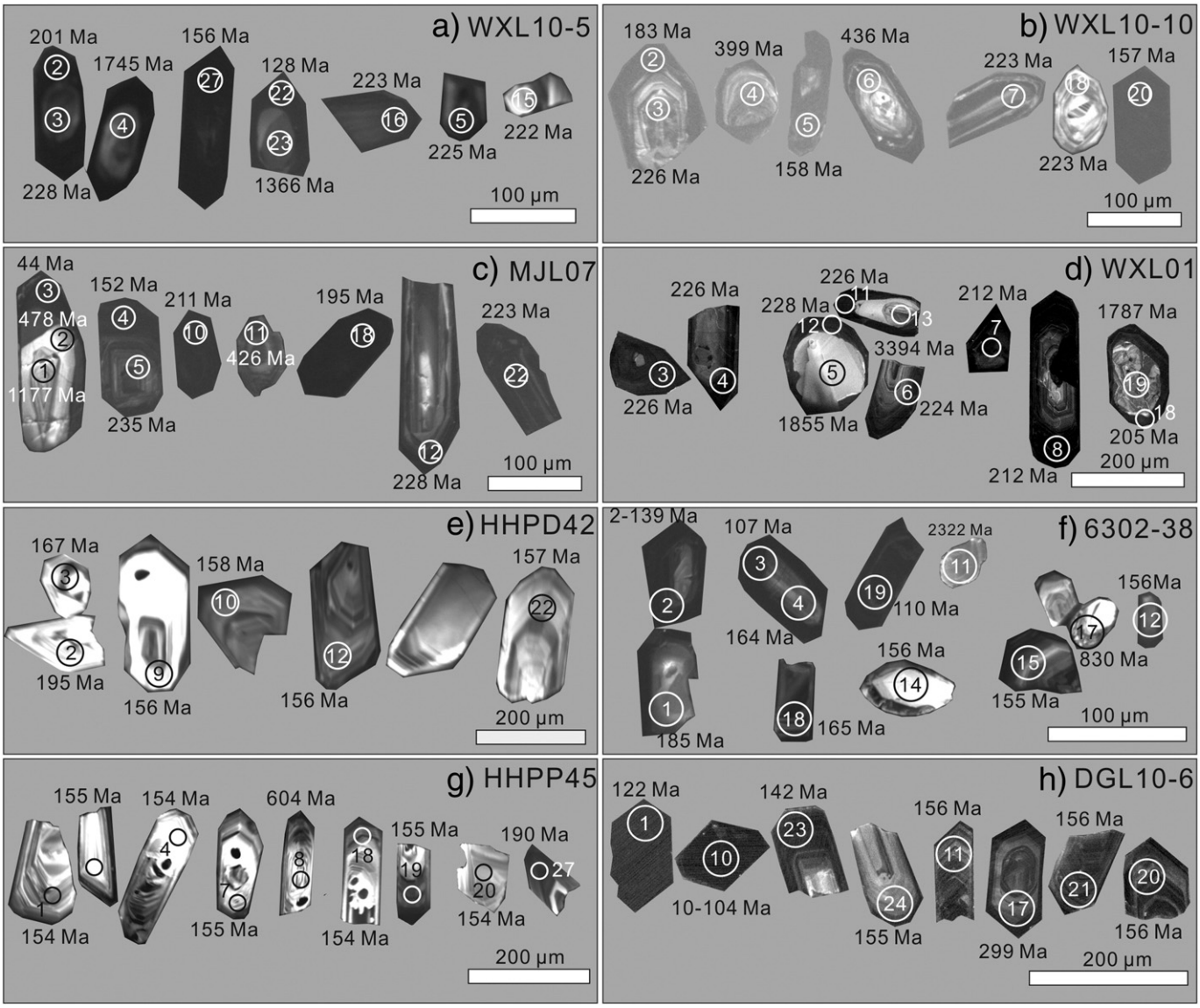

Fig. 9. Representative cathodoluminescence images for zircons from granitic rocks in the Wangxianling area.

of 191 Ma and 895 Ma. The remaining 25 grains have U contents and Th/U ratios ranging from 216 to 4100 ppm and 0.14 to 0.55, respectively, and yield a weighted mean $^{206}Pb/^{238}U$ age of 157.1 ± 0.8 Ma (MSWD = 0.4). This age is interpreted as the crystallization age of the sample. A total of 26 spots on 24 zircon grains were measured for sample 6302-38 (Fig. 10f). Eight zircons with mostly dark CL images and high U contents (up to 49,800 pm) give younger $^{206}Pb/^{238}U$ ages from 79 to 140 Ma, and are therefore rejected as a result of Pb loss. The $^{206}Pb/^{238}U$ ages of two inherited cores are 185 Ma and 164 Ma, and of four inherited grains are 2322 Ma, 830 Ma, 406 Ma, and 165 Ma. Twelve grains yield a weighted mean $^{206}Pb/^{238}U$ age of 155.3 ± 1.2 Ma (MSWD = 1.2) representing the crystallization age of the sample. The above results suggest that the Hehuaping pluton crystallized at ~156 Ma.

4.1.3. Granite porphyry dykes

Most zircon grains in the granite porphyry dykes are colorless, and have clear CL images with unambiguous oscillatory zoning (Fig. 9g, h). Some grains are faint yellow and brown, and have blurry CL textures. A few zircon grains containing thorite inclusions show metamict textures. Thirty-one zircon grains were analyzed for sample HHPP45 (Fig. 10g). One inherited grain has a $^{206}Pb/^{238}U$ age of 604 Ma. Two grains (HHPP45-27 and HHPP45-28) have discordant U–Pb ages and are rejected. Twenty-eight zircon grains have low Th and U contents, and Th/U ratios, ranging from 53 to 450 ppm, 187 to 1270 ppm and 0.35 to 0.90, respectively. $^{206}Pb/^{238}U$ ages for these grains range from 154 to 156 Ma and yield a weighted mean age of 154.9 ± 0.5 Ma (MSWD = 0.15) representing the crystallization age of the sample. A total of 25 spots on 25 grains were analyzed for sample DGL10-6 (Fig. 10h). Analytical spot DGL10-6-17 had a discordant U–Pb age and was rejected. Two dark zircons with high U contents (15100 ppm and 32200 ppm) have concordant and younger ages of 104 Ma and 122 Ma, respectively. One zircon grain (DGL10-6-23) with blurry oscillatory zoning has a younger $^{206}Pb/^{238}U$ age of 142 Ma. These three younger ages are rejected. Twenty-one grains have Th and U concentrations varying from 196 to 2128 ppm and 463 to 5127 ppm, respectively, and Th/U ratios from 0.26 to 0.50. Their weighted mean $^{206}Pb/^{238}U$ age is 157.3 ± 0.8 Ma (MSWD = 1) representing the crystallization age of the sample. Base on the dating results of HHPP45 and DGL10-6, the granite porphyry dykes are interpreted to have been intruded at ~156 Ma.

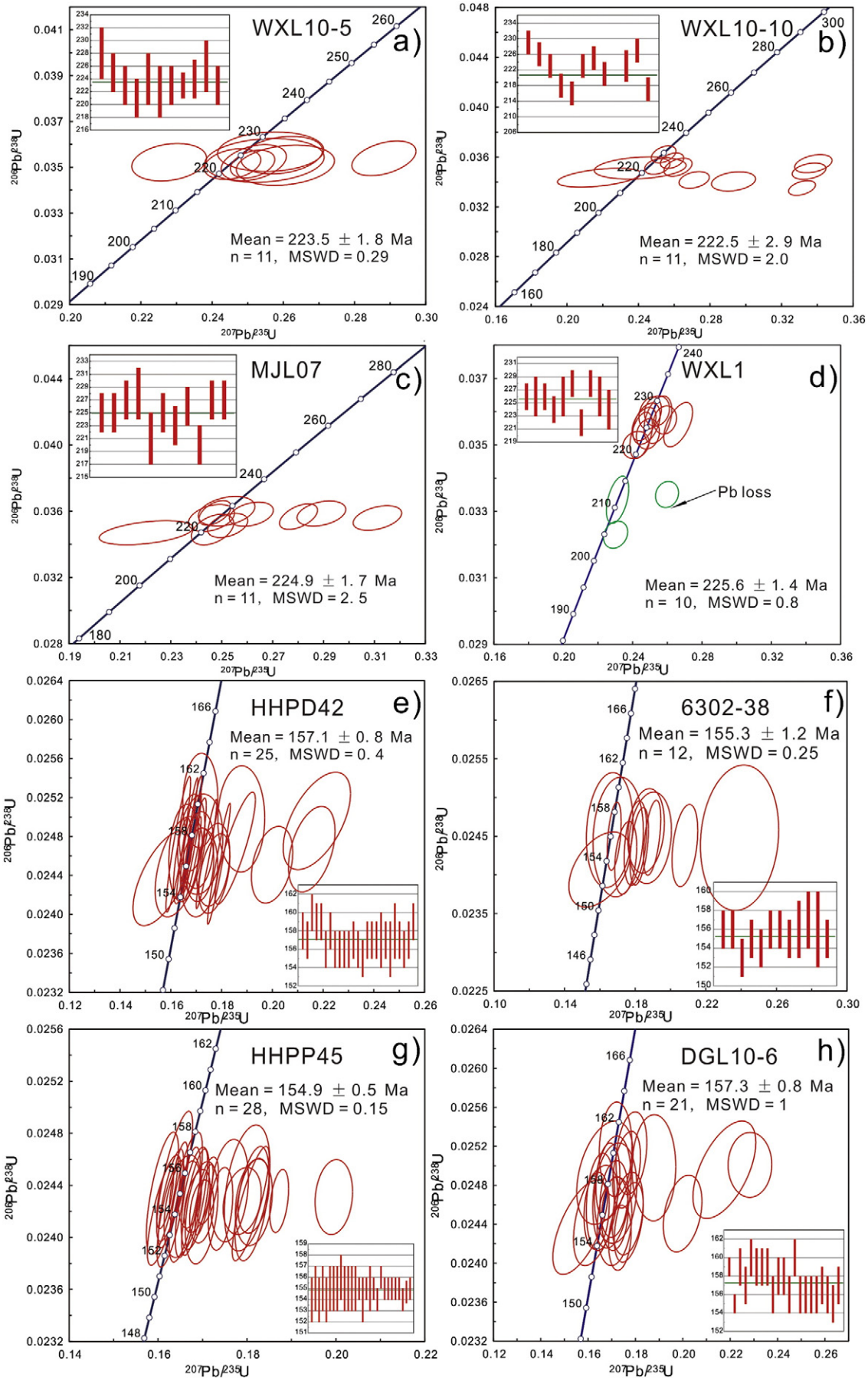

Fig. 10. Zircon U–Pb concordia diagrams for granitic rocks in the Wangxianling area.

Table 4
Re–Os isotope compositions for molybdenites from the tungsten-bearing quartz veins in the Shuiyuanshan and Yejiwo tungsten deposits.

Sample	weight (g)	Re (ng/g)	2σ	C_{Os} (ng/g)	2σ	^{187}Re (ng/g)	2σ	^{187}Os (ng/g)	2σ	Age(Ma)	2σ
Shuiyuanshan tungsten deposit											
10WXL38-1	0.02372	6588	51	0.0023	0.1364	4141	32	15.10	0.15	218.5	3.3
10WXL28	0.05806	8220	64	0.0037	0.0165	5167	40	19.19	0.17	222.5	3.2
10WXL32-1	0.05035	6345	52	0.0096	0.0101	3988	33	14.70	0.13	220.8	3.2
10WXL32-2	0.05006	5385	48	0.0140	0.0097	3384	30	12.51	0.10	221.4	3.2
10WXL32-9	0.05326	3942	35	0.0043	0.0144	2477	22	9.148	0.077	221.2	3.2
10WXL33	0.05088	4867	39	0.0043	0.0097	3059	24	11.25	0.10	220.4	3.2
10WXL38-2	0.05053	7507	61	0.0099	0.0209	4718	38	17.31	0.16	219.9	3.2
10WXL39	0.05033	4904	43	0.0181	0.0233	3082	27	11.30	0.09	219.7	3.2
Yejiwo tungsten deposit											
12YJW07	0.01508	8724	78	0.205	0.051	5483	49	20.63	0.18	225.4	3.3
12YJW08	0.01517	5084	48	0.060	0.059	3195	30	12.08	0.11	226.5	3.5
12YJW09	0.01527	35803	314	0.030	0.017	22503	198	85.87	0.68	228.6	3.3
12YJW10	0.01513	6439	59	0.056	0.017	4047	37	15.41	0.13	228.1	3.4
12YJW11	0.01506	14482	123	0.035	0.040	9102	77	34.53	0.31	227.3	3.3

Cos: Common Os

4.2. Molybdenite Re–Os ages of the tungsten deposits

Eight molybdenite separates from wolframite–quartz veins in the Shuiyuanshan tungsten deposit were analyzed for the Re and Os isotopic compositions, and are listed in Table 4. The Re and ^{187}Os contents of molybdenite separates range from 3.94 to 8.22 ppm and 9.15 to 19.19 ppm, respectively. They have relatively tight Re–Os model ages from 218.5 ± 3.3 to 222.5 ± 3.2 Ma, with a weighted mean age of 220.6 ± 1.1 Ma (MSWD = 0.59). These samples yield a ^{187}Re–^{187}Os isochron age of 220.7 ± 4.1 Ma (MSWD = 1.0) which agrees well with the weighted mean age (Fig. 11a, b).

Five molybdenite separates from quartz–tourmaline veins in the Yejiwo tungsten deposit were measured. The Re and ^{187}Os contents vary from 5.08 to 35.80 ppm and 12.08 to 85.87 ppm, respectively. The molybdenite separates have relatively tight Re–Os model ages from 225.4 ± 3.3 to 228.6 ± 3.4 Ma, with a weighted mean age of 227.2 ± 1.5 Ma (MSWD = 0.6). These samples yield a well-constrained ^{187}Re–^{187}Os isochron age of 228.1 ± 2.6 Ma (MSWD = 0.9), which is in good accordance with the weighted mean age (Fig. 11c, d).

4.3. Muscovite ^{40}Ar–^{39}Ar age of the tungsten deposit

^{40}Ar–^{39}Ar analytical results for muscovite from the Shuiyuanshan tungsten deposit (sample WXL-2) are presented in Table 5 and illustrated in Fig. 12. The ^{40}Ar–^{39}Ar muscovite steps yield a plateau age of 214.3 ± 1.1 Ma based on 86.6% released ^{39}Ar. Regressing the most radiogenic steps through the composition of atmospheric argon (^{40}Ar/^{36}Ar = 295.5) on an inverse isochron diagram yields an age of 214.2 ± 2.9 Ma (MSWD = 1.9), and this is consistent with the plateau age.

4.4. Cassiterite U–Pb ages of the tin deposit

Cassiterite grains are yellow to brown and a few contain inclusions and cracks. U–Pb isotopic analyses were conducted on the areas where there are no inclusions and cracks. The analytical results are presented in Table 6.

Twenty-seven cassiterite separates were analyzed for sample WXL-17 from the tin greisen. Ratios of ^{238}U/^{207}Pb and ^{206}U/^{207}Pb show a large variation, ranging from 4.15 to 69.35 and 1.21 to 19.96, respectively. After correction for common Pb, the analyses yield a reliable ^{206}Pb/^{207}Pb–^{238}U/^{207}Pb isochron age of 154.8 ± 5.8 Ma (MSWD = 0.6) with an initial ^{206}Pb/^{207}Pb ratio of 1.1747. This age represents the mineralization age of the tin greisen (Fig. 13a).

Forty-eight cassiterite grains separated from two tin skarn samples (IV-1 and IV-2) were analyzed and evaluated using one isochron. These grains are characterized by variable ^{238}U/^{207}Pb and ^{206}U/^{207}Pb ratios ranging from 0.21 to 53.39 and 1.19 to 2.61, respectively. One well-constrained and credible ^{206}Pb/^{207}Pb–^{238}U/^{207}Pb isochron age of 157.8 ± 4.1 Ma (MSWD = 7.8) was obtained with an initial ^{206}Pb/^{207}Pb ratio of 1.1736. This age may represent the formation age of the tin skarn (Fig. 13b).

5. Discussion

5.1. Timing of granitic magmatism in the Wangxianling area

Many zircon grains from the Wangxianling granite are characterized by abundant uraninite inclusions and fractures, and high U contents. Oscillatory zoning in these grains is not clear, and this is possibly a result of metamictization and recrystallization (Fig. 9). They commonly have U–Pb apparent ages ranging from 56.7 to 212 Ma, which are younger than ages for the grains without metamictization. Weak greisenization of the Wangxianling granite might have allowed leaching of Pb in the metamict zircon, resulting in younger ages. Thus, zircons with high U and Th contents from the Wangxianling granite, which give younger ages, should therefore be excluded from the calculation of the weighted mean age.

The emplacement age of the Wangxianling pluton has been contentious. Previous published results by muscovite K–Ar and zircon U–Pb dating gave ages from 206 to 235 Ma (Geologic Team of Southern Hunan Province, 1983; Wei et al., 2007; Zheng and Guo, 2012), which do not better match one to another within their analytical errors. Our new *in situ* zircon U–Pb ages of four samples from the central and marginal phases of the Wangxianling pluton range from 222.5 ± 2.9 to 225.6 ± 1.4 Ma, averaging ~224 Ma. This age is consistent with the oldest K–Ar age (222.5 Ma) but is different from the two published zircon U–Pb ages (212 Ma and 235 Ma). During the field investigation, no other granite types were observed in the Wangxianling granite pluton. We contend that our four samples for zircon U–Pb dating were representatively collected from different locations in the Wangxianling pluton, and therefore, it can be concluded that the Wangxianling pluton was emplaced at ~224 Ma.

Fine-grained Hehuaping biotite granite cuts the eastern marginal phase of the Wangxianling pluton and was originally thought to be a Late Triassic supplementary phase of the pluton (Geologic Team of Southern Hunan Province, 1983). However, Zheng and Guo (2012) reported a zircon U–Pb age of 155.9 ± 1.0 Ma for a biotite granite sample in the northeast of the Wangxianling pluton. Our zircon U–Pb ages for

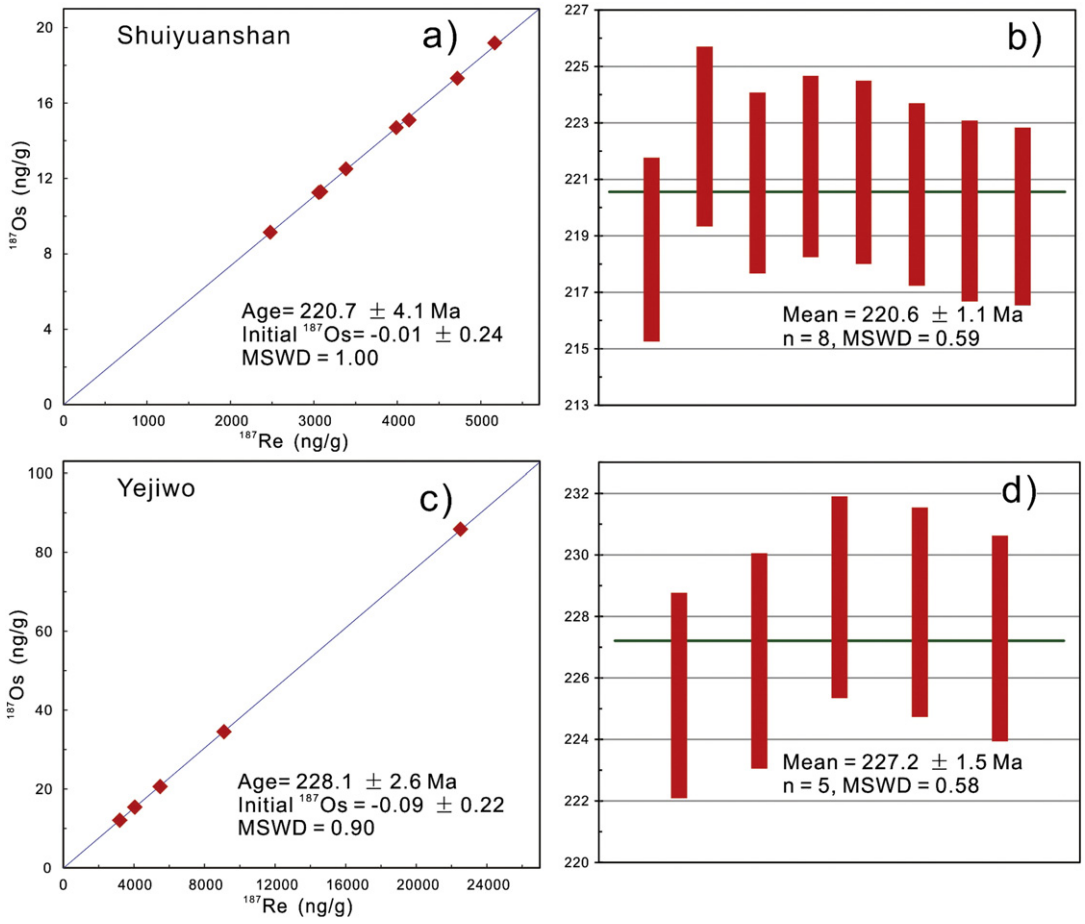

Fig. 11. Re–Os isochron and weighted average model age diagrams for molybdenites from the Shuiyuanshan (a and b) and Yejiwo (c and d) tungsten deposits.

two biotite granite samples from two drill holes in the Hehuaping tin deposit are 157.1 ± 0.8 Ma and 155.3 ± 1.2 Ma. Collectively, these three ages are consistent within analytical error, and are interpreted to represent the crystallization age (~156 Ma) of the Hehuaping biotite granite pluton (Fig. 14).

Wei et al. (2007) reported a zircon U–Pb age of 159 ± 3 Ma for a granite porphyry dyke. Our zircon U–Pb ages from two granite porphyry dykes are 154.9 ± 0.5 Ma and 157.4 ± 0.8 Ma, which indicate that the dykes were emplaced at ~156 Ma.

5.2. Timing of W and Sn mineralization in the Wangxianling area

Cai et al. (2006) reported a molybdenite Re–Os isochron age of 224.0 ± 1.9 Ma and interpreted it as the timing of Sn mineralization in the Hehuaping deposit. However, the samples were not clearly described. In the present study, five molybdenite samples were obtained from tourmaline–quartz veins crosscutting the Wangxianling granite in the Yejiwo tungsten deposit, and these samples yield a Re–Os isochron age of 228.1 ± 2.6 Ma. This age, associated with W mineralization,

Table 5
^{40}Ar–^{39}Ar isotopic analytical results for the scheelite greisen from the Shuiyuanshan tungsten deposit.

T (°C)	$^{40}Ar/^{39}Ar$	$^{37}Ar/^{39}Ar$	$^{36}Ar/^{39}Ar$	$^{40}Ar^*/^{39}Ar_k$	$^{40}Ar^*$ (%)	$^{39}Ar_k$ (%)	Age (Ma)	2σ
WXL-02, muscovite, J = 0.0043400 ± 0.0000109								
750	26.61333	0.01070	0.01668	21.686346	81.49	0.30	162.66	2.73
800	29.87381	0.00671	0.01534	25.342514	84.83	0.92	188.69	2.49
850	30.11463	0.00038	0.00639	28.226196	93.73	8.53	208.97	1.06
880	29.16558	0.00041	0.00081	28.924953	99.17	19.09	213.85	1.06
910	29.02223	0.00024	0.00052	28.869263	99.47	29.46	213.46	0.93
940	29.28634	0.00032	0.00050	29.138621	99.50	19.83	215.34	1.02
970	29.16936	0.00042	0.00063	28.983025	99.36	8.81	214.25	0.93
1000	29.24137	0.00050	0.00079	29.006460	99.20	4.35	214.42	0.96
1030	29.38230	0.00014	0.00090	29.117287	99.10	2.71	215.19	1.47
1070	29.22279	0.00064	0.00080	28.986259	99.19	2.40	214.28	1.00
1110	29.34108	0.00249	0.00081	29.102992	99.19	2.02	215.09	1.93
1160	29.70892	0.00495	0.00147	29.276028	98.54	1.09	216.29	1.68
1260	31.05631	0.00324	0.00558	29.406625	94.69	0.47	217.20	2.65

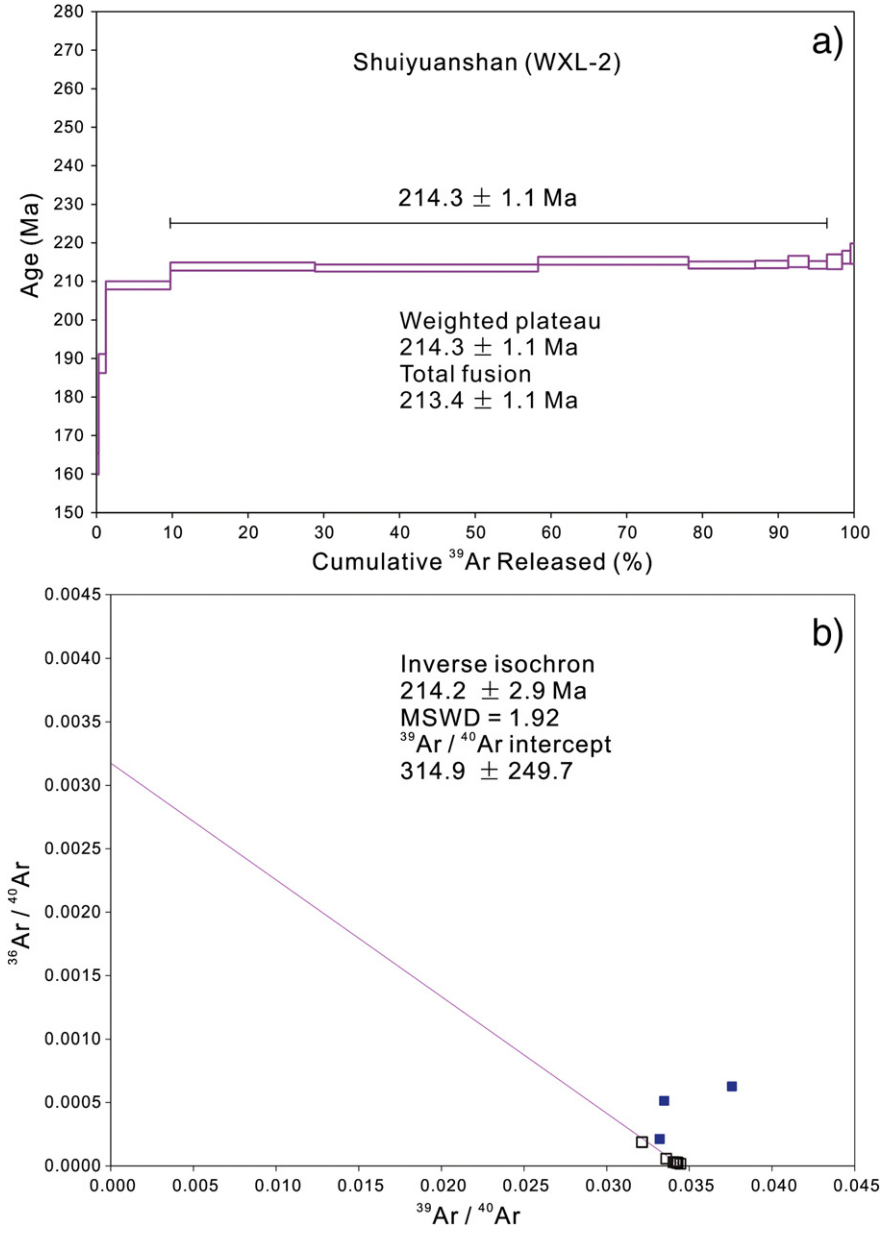

Fig. 12. Muscovite ^{40}Ar–^{39}Ar plateau age (a) and inverse isochron age (b) plots for the scheelite greisen in the Shuiyuanshan tungsten deposit.

is similar to the Re–Os isochron age of Cai et al. (2006). Eight molybdenite samples from the quartz–wolframite veins in the Shuiyuanshan tungsten deposit have a Re–Os isochron age of 220.7 ± 4.1 Ma. The muscovite ^{40}Ar–^{39}Ar date of scheelite greisen from the Shuiyuanshan deposit is 214.3 ± 1.1 Ma. Collectively, these Late Triassic isotopic ages are thought to represent the timing of W mineralization rather than the timing of Sn mineralization.

Cassiterite is the dominant ore mineral in tin deposits and has a countable U content. It generally remains stable and is not easily affected by late hydrothermal events (Gulson and Jones, 1992; Jiang et al., 2004). Thus, the U–Pb age of cassiterite may help constrain the timing of Sn mineralization. The first precise cassiterite U–Pb dating by single-grain chemical abrasion was used to constrain the mineralization ages of Zaaiplaats tin deposit in South Africa and the Belitung tin deposit in Indonesia (Gulson and Jones, 1992). Cassiterite U–Pb dating was also carried out by Yuan et al. (2008) and Liu et al. (2007) using single-grain chemical abrasion and by Yuan et al. (2011) using *in situ* isotope dating by LA-ICP-MS. Our *in situ* U–Pb dating of the cassiterite from the tin greisen and tin skarn in the Hehuaping deposit yields an average age of ~156 Ma, which is interpreted as the timing of Sn mineralization. This age differs significantly from the W mineralization that we infer, and suggests W and Sn mineralization in the Wangxianling area were formed in different times: the W mineralization occurred at ~224 Ma, whereas the Sn mineralization took place at ~156 Ma. This implies that Sn mineralization is ~70 My younger than the W mineralization.

5.3. Genetic relationships between granitic magmatism and W–Sn mineralization

Tungsten mineralization occurs in the Wangxianling pluton and in the adjacent strata that the pluton intrudes, whereas tin mineralization occurs in the granite porphyry dykes and in the surrounding rocks that the dykes and the Hehuaping pluton intrude. Mineralogically, geochemically and isotopically, the granite of the Wangxianling pluton is a highly fractionated S-type granite and is similar to the typical S-type

Table 6
In situ LA-ICP-MS cassiterite U-Pb dating results for the tin greisen and tin skarn in the Hehuaping tin deposit.

Sample	$^{238}U/^{207}Pb$	error % (1σ)	$^{206}Pb/^{207}Pb$	error % (1σ)	$^{206}Pb/^{238}U$	error % (1σ)
Tin greisen						
WXL-17.1	27.90	6.29	1.88	3.01	0.105204	4.13
WXL-17.2	6.24	1.21	1.32	0.19	0.220049	1.79
WXL-17.3	16.30	2.78	1.58	0.87	0.120202	4.29
WXL-17.4	10.65	4.91	1.44	1.29	0.213562	5.24
WXL-17.6	10.93	1.63	1.44	0.62	0.138169	1.57
WXL-17.7	39.60	7.50	2.28	4.92	0.090246	4.59
WXL-17.8	5.89	2.39	1.32	0.49	0.278500	5.17
WXL-17.10	24.25	4.57	1.74	1.35	0.097818	4.52
WXL-17.11	8.68	4.02	1.38	0.79	0.236726	4.78
WXL-17.12	8.90	1.98	1.39	0.39	0.170281	2.22
WXL-17.13	26.39	4.74	1.82	1.86	0.099357	4.43
WXL-17.14	13.70	3.34	1.53	1.21	0.142409	4.12
WXL-17.15	2.57	1.66	1.24	0.20	0.520110	2.30
WXL-17.16	27.94	6.40	1.90	3.05	0.118028	5.91
WXL-17.17	28.39	19.96	2.00	11.66	0.237950	8.27
WXL-17.18	31.26	5.57	1.96	2.53	0.119323	6.65
WXL-17.19	69.35	13.04	2.98	9.85	0.127747	8.09
WXL-17.20	18.83	2.77	1.63	0.88	0.101752	3.03
WXL-17.22	9.72	3.88	1.42	0.81	0.226069	5.77
WXL-17.23	5.48	5.47	1.32	0.73	0.439456	5.29
WXL-17.24	5.57	5.69	1.33	1.58	0.407640	5.59
WXL-17.25	38.19	17.47	2.28	11.04	0.114726	6.59
WXL-17.26	7.93	1.40	1.37	0.22	0.179008	1.38
WXL-17.27	6.31	5.16	1.34	1.38	0.360037	5.82
WXL-17.28	5.56	2.84	1.31	0.39	0.296474	3.93
WXL-17.29	24.79	7.21	1.78	2.92	0.198451	8.57
WXL-17.30	4.15	2.48	1.28	0.31	0.361900	3.43
Tin skarn						
IV-1.1	15.94	6.51	1.58	2.59	0.348579	10.64
IV-1.2	31.29	4.87	1.94	2.21	0.094589	5.66
IV-1.3	2.98	4.40	1.24	0.38	0.797854	8.80
IV-1.4	53.39	10.10	2.61	6.51	0.122877	10.95
IV-1.5	1.91	1.38	1.22	0.38	0.665615	1.62
IV-1.7	24.10	4.04	1.76	1.58	0.091810	3.08
IV-1.8	42.78	7.10	2.28	4.01	0.084992	4.56
IV-1.9	14.74	3.33	1.56	1.25	0.127204	3.07
IV-1.10	40.27	4.62	2.19	2.45	0.079873	5.67
IV-1.11	0.32	0.60	1.18	0.03	3.721769	0.58
IV-1.12	1.96	4.00	1.22	0.31	0.939819	5.38
IV-1.13	7.90	2.41	1.36	0.40	0.196509	2.81
IV-1.14	19.20	4.16	1.63	1.22	0.132201	6.18
IV-1.15	6.13	1.68	1.32	0.29	0.229525	2.04
IV-1.16	2.50	1.60	1.23	0.24	0.523322	1.91
IV-1.17	33.55	2.50	2.02	1.22	0.065875	2.00
IV-2.4	0.61	4.07	1.19	0.56	2.830113	5.11
IV-2.6	0.65	2.17	1.24	1.37	2.127593	3.10
IV-2.8	0.21	5.97	1.19	0.90	5.718002	3.82
IV-2.9	0.40	1.51	1.18	0.58	3.142736	2.10
IV-2.11	0.68	4.98	1.20	1.22	3.592014	13.64
IV-2.12	0.35	2.68	1.19	0.55	7.013583	16.74
IV-2.13	0.41	1.04	1.19	0.41	2.968670	1.19
IV-2.14	0.51	2.98	1.20	0.75	2.852055	3.57
IV-2.16	0.46	1.37	1.19	0.02	2.675697	1.21
IV-2.17	0.13	1.17	1.18	0.02	9.265035	0.96
IV-2.18	5.72	3.25	1.33	0.49	0.275339	2.61
IV-2.19	5.57	2.99	1.33	0.42	0.290264	3.32
IV-2.20	35.07	4.95	2.12	2.51	0.077223	2.79
IV-2.21	0.64	1.29	1.19	0.03	1.934176	1.46
IV-2.23	0.84	0.95	1.20	0.04	1.456824	0.91
IV-2.24	0.43	0.45	1.18	0.05	2.785204	0.46
IV-2.27	3.27	2.45	1.26	0.30	0.459878	3.67
IV-2.28	1.36	0.52	1.21	0.07	0.896760	0.50
IV-2.29	0.32	0.52	1.18	0.02	3.724384	0.51
IV-2.30	0.70	0.92	1.19	0.03	1.726524	0.90
IV-2.32	0.86	1.46	1.20	0.04	1.453503	1.54
IV-2.33	0.57	0.71	1.19	0.04	2.104774	0.70
IV-2.34	1.17	1.85	1.20	0.10	1.088915	1.59

tungsten-bearing granites in the Nanling Range (Chen et al., 2008). Greisenization of the Wangxianling granite is common, and is associated with high tungsten contents (up to 380 ppm). The ~224 Ma Wangxianling pluton hosts tungsten-mineralized veins with an average Re–Os age of ~224 Ma and scheelite greisen with an muscovite ^{40}Ar–^{39}Ar age of 214.3 ± 1.1 Ma. Thus, the W mineralization event in the Wangxianling area is spatially and temporally related to the Late Triassic Wangxianling granite pluton.

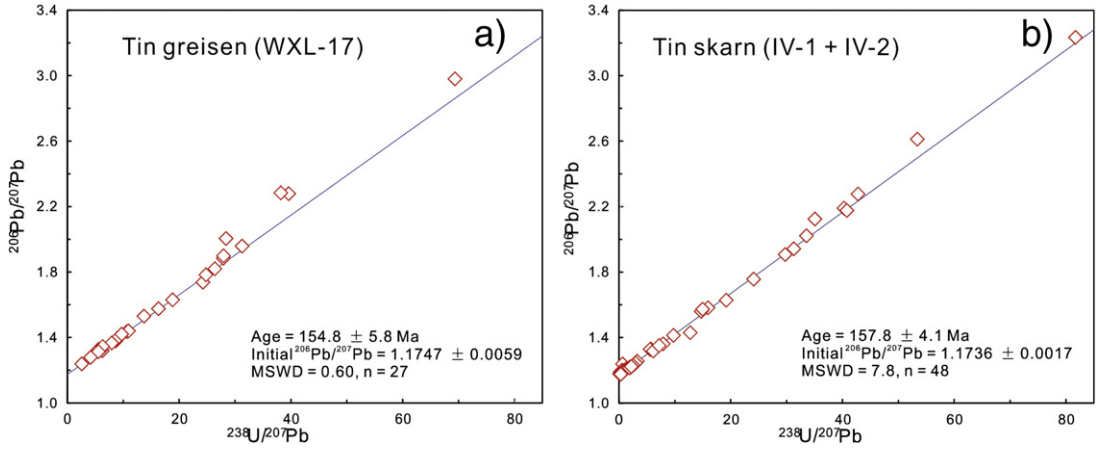

Fig. 13. Cassiterite U–Pb isochron diagrams for the tin greisen (a) and tin skarn (b).

Both the Hehuaping biotite granite pluton and granite porphyry dykes have affinities of A_2-type granite and are similar to the Sn-bearing granites in the western Nanling Range. *In situ* cassiterite U–Pb age (156 Ma) of the tin greisen and skarn indicate a younger Sn mineralization event in the Wangxianling area. The time of this event is consistent with the ~156 Ma Hehuaping pluton and granite porphyry dykes. Hence, the Sn mineralization in the Wangxianling area is inferred to be associated with the Late Jurassic Hehuaping pluton and granite porphyry dykes.

5.4. Implications for regional metallogeny in the Nanling Range

There are two important periods of Mesozoic magmatism in the Nanling Range: the Triassic (251–205 Ma) and the Middle–Late Jurassic (180–142 Ma) (Zhou et al., 2006). Tungsten deposits discovered in the Nanling Range are dominantly associated with the Late Jurassic S-type granite. The Triassic granites are mainly distributed in the middle and western Nanling Range, far from the continental margin (Chen and Jahn, 1998; Wang et al., 2007). Sixty percent of them are strongly peraluminous granites and contain aluminous minerals such as muscovite, garnet and tourmaline that are characteristic of S-type granites (Sun et al., 2005). In recent years, and with the advent of high-precision isotopic dating, more attention has been paid to tungsten deposits and their relationship to Late Triassic granites. Feng et al. (2013) obtained a muscovite ^{40}Ar–^{39}Ar isochron age (212.4 ± 1.4 Ma) for greisen in the Limu W–Sn–Nb–Ta district, which overlaps with the zircon U–Pb ages (218.3 ± 2.2 Ma and 214 ± 5 Ma) of the Limu granite. The Re–Os isochron age for W (Sn) mineralization in Liguifu is 211.9 ± 6.4 Ma, and this overlaps with the zircon U–Pb age (215 Ma) of biotite granite in the central Dupangling composite granite in Guangxi Province (Gan, 1990; Zou et al., 2009). Wu et al. (2012) published a molybdenite Re–Os isochron age of 216.8 ± 7.5 Ma for the Yuntoujie W–Mo deposit, which is similar to the zircon U–Pb age of 216.8 ± 4.9 Ma for the muscovite granite found in the Miaoershan–Yuechengling complex of the western Nanling Range. Our new Late Triassic ages obtained for both the Wangxianling pluton and its associated W mineralization also demonstrate a similarity, and imply an association between Late Triassic granitic magmatism and W mineralization. Hence, it is suggested here that the Late Triassic granites in the Nanling Range have great potential for W mineralization. Further detailed studies of Late Triassic W mineralization and prospecting for economic ore deposits around the Late Triassic granites should be strongly encouraged.

Late Jurassic tin-bearing granites are mainly distributed in the western and middle Nanling Range as a NE-trending granitic belt (Chen et al., 2008; Jiang et al., 2006; Zhao et al., 2012; Zhu et al., 2008). Generally, these tin-bearing granites have few inherited zircons and high zircon

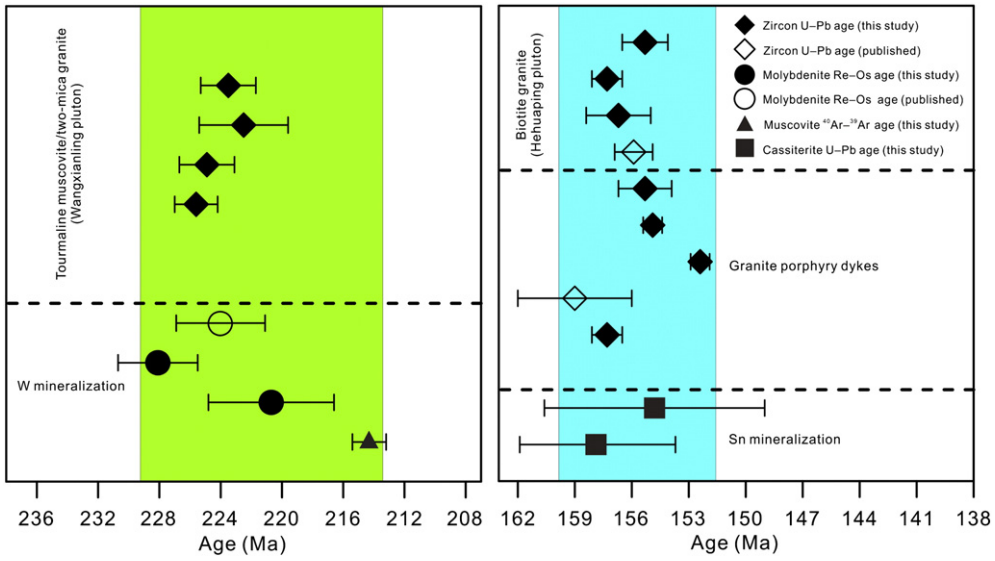

Fig. 14. Age spectra incorporating granitic rocks, W and Sn deposits in the Wangxianling area. The published zircon U–Pb ages are from Wei et al. (2007) and Zheng and Guo (2012) and the published molybdenite Re–Os age is from Cai et al. (2006).

saturation temperatures (>800 °C), and are classed as high-temperature granites (Huang et al., 2011; Zhu et al., 2010). They are characterized by elevated Zr + Nb + Ce + Y (>340 ppm) and REE contents, flat REE patterns, high 10000*Ga/Al ratios (>2.6), relatively high ε_{Nd} and ε_{Hf} values and young two-stage model ages, all of which are typical of A_2-type granites (Chen et al., 2008; Fu et al., 2005; Huang et al., 2011; Jiang et al., 2006, 2009; Wang et al., 2014; Zhao et al., 2010, 2012; Zhou et al., 2013; Zhu et al., 2008). The Late Jurassic Hehuaping biotite pluton and granite porphyry dykes of this study, both of which are associated with Sn mineralization, also lie within the NE-trending granitic belt and have geochemical characteristics of A_2-type granites. Collectively, these A_2-type tin-bearing granites are distinctly from the S-type tungsten-bearing granites in the Nanling Range (such as the Wangxianling pluton). Hence, tin prospecting in the Nanling Range should focus on the Late Jurassic A_2-type granites.

6. Conclusions

1. Zircon U–Pb dating results illustrate that the Wangxianling pluton was emplaced at ~224. The hidden Hehuaping pluton and granite porphyry dykes were emplaced at ~156 Ma.
2. Molybdenite Re–Os and muscovite ^{40}Ar–^{39}Ar dating at both the Shuiyuanshan and Yejiwo tungsten deposits shows that W mineralization took place during the Late Triassic. *In situ* LA-ICP-MS U–Pb dating for cassiterite from both the tin greisen and tin skarn in the Hehuaping deposit confirms a Late Jurassic age for Sn mineralization.
3. In the Wangxianling area, the Late Triassic W mineralization is associated with the ~224 Ma Wangxianling S-type granite pluton, whereas the Late Jurassic Sn mineralization is associated with the ~156 Ma Hehuaping A_2-type granite pluton and the ~156 Ma A_2-type granite porphyry dykes.

Acknowledgements

This study was supported by the National Science Foundation of China (41273053 and 41302072) and the Major State Basic Research Development Program of China (2012CB416702). The authors thank Hui-Min Li at the Tianjing Institute of Geology and Mineral Resources, Ke-Jun Hou at the Chinese Academy of Geological Sciences in Beijing and Liang Li at the Institute of Geochemistry, CAS, Guiyang, for their technical assistances with the cassiterite and zircon U–Pb analyses. Mei-Fu Zhou, Bernd Lehmann, Jian-Wei Li and Xin-Guang Wang are thanked for their comments and improvements to the manuscript.

References

Andersen, T., 2002. Correction of common lead in U-Pb analyses that do not report ^{204}Pb. Chem. Geol. 192, 59–79.

Bai, X.J., Wang, M., Jiang, Y.D., Qiu, H.N., 2013. Direct dating of tin-tungsten mineralization of the Piaotang tungsten deposit, South China, by $^{40}Ar/^{39}Ar$ progressive crushing. Geochim. Cosmochim. Acta 114, 1–12.

Bell, K., Anglin, C., Franklin, J., 1989. Sm-Nd and Rb-Sr isotope systematics of scheelites: Possible implications for the age and genesis of vein-hosted gold deposits. Geology 17, 500–504.

Black, L.P., Gulson, B.L., 1978. The age of the Mud Tank carbonatite, Strangways Range, Northern Territory. BMR J. Aust. Geol. Geophys. 3, 227–232.

Cabral, A.R., Eugster, O., Brauns, M., Lehmann, B., Rösel, D., Zack, T., de Abreu, F.R., Pernicka, E., Barth, M., 2013. Direct dating of gold by radiogenic helium: Testing the method on gold from Diamantina, Minas Gerais, Brazil. Geology 41, 163–166.

Cai, M.H., Chen, K.X., Qu, W.J., Liu, G.Q., Fu, J.M., Yin, J.P., 2006. Geological characteristics and Re-Os dating of molybdenites in Hehuaping tin-polymetallic deposit, southern Hunan Province. Mineral Deposits 25, 263–268 (in Chinese with English abstract).

Che, X.D., Wu, F.Y., Wang, R.C., Gerdes, A., Ji, W.Q., Zhao, Z.H., Yang, J.H., Zhu, Z.Y., 2014. In situ U–Pb isotopic dating of columbite-tantalite by LA-ICP-MS. Ore Geol. Rev. http://dx.doi.org/10.1016/j.oregeorev.2014.07.008.

Chen, J.F., Jahn, B.M., 1998. Crustal evolution of southeastern China: Nd and Sr isotopic evidence. Tectonophysics 284, 101–133.

Chen, J., Lu, J.J., Chen, W.F., Wang, R.C., Ma, D.S., Zhu, J.C., Zhang, W.L., Ji, J.F., 2008. W-Sn-Nb-Ta-Bearing granites in the Nanling Range and their relationship to metallogenesis. Geol. J. China Univ. 14, 459–473 (in Chinese with English abstract).

Chen, J., Wang, R.C., Zhu, J.C., Lu, J.J., Ma, D.S., 2013. Multiple-aged granitoids and related tungsten-tin mineralization in the Nanling Range, South China. Sci. Chin.Earth Sci. 56, 2045–2055.

Du, A.D., Zhao, D.M., Wang, S.X., Sun, D.Z., Liu, D.Y., 2001. Precise Re-Os dating for molybdenite by ID-NTIMS with carius tube sample preparation. Rock Min. Anal. 20, 247–252.

Du, A.D., Wu, S.Q., Sun, D.Z., Wang, S.X., Qu, W.J., Markey, R., Stein, H., Morgan, J., Malinovskiy, D., 2004. Preparation and certification of Re-Os dating reference materials: Molybdenites HLP and JDC. Geostand. Geoanal. Res. 28, 41–52.

Feng, Z.H., Kang, Z.Q., Yang, F., Liao, J.F., Wang, C.Z., 2013. Geochronology of the Limu W-Sn-Nb-Ta-bearing granite pluton in South China. Resour. Geol. 63, 320–329.

Fu, J.M., Ma, C.Q., Xie, C.F., 2005. Ascertainment of the Jinjiling aluminous A-type granite, Hunan Province and its tectonic settings. Geochimica 34, 215–226 (in Chinese with English abstract).

Gan, G.L., 1990. Basic characters and petrogenesis of the Dupangling granite. Jiangxi Geol. 3, 15–30 (in Chinese with English abstract).

Geologic Team of Southern Hunan Province, 1983. 1:50000 regional geology survey report of Chen county: Geology volume, 159 pp (in Chinese).

Gulson, B.L., Jones, M.T., 1992. Cassiterite: Potential for direct dating of mineral deposits and a precise age for the Bushveld Complex granites. Geology 20, 355–358.

Hall, C.M., Walter, R.C., Westgate, J.A., York, D., 1984. Geochronology, stratigraphy and geochemistry of Cindery tuff in Pliocene hominid-bearing sediments of the Middle Awash, Ethiopia. Nature 308, 26–31.

He, Z.Y., Xu, X.S., Zou, H.B., Wang, X.D., Yu, Y., 2010. Geochronology, petrogenesis and metallogeny of Piaotang granitoids in the tungsten deposit region of South China. Geochem. J. 44, 299–313.

Hou, K.J., Li, Y.H., Tian, Y.Y., 2009. *In situ* U-Pb zircon dating using laser ablation-multi ion counting-ICP-MS. Mineral Deposits 28, 481–492 (in Chinese with English abstract).

Hu, R.Z., Zhou, M.F., 2012. Multiple Mesozoic mineralization events in South China: An introduction to the thematic issue. Mineral. Deposita 47, 579–588.

Hu, Z.C., Liu, Y.D., Chen, L., Zhou, L., Li, M., Zong, K.Q., Zhu, L.Y., Gao, S., 2011. Contrasting matrix induced elemental fractionation in NIST SRM and rock glasses during laser ablation ICP-MS analysis at high spatial resolution. J. Anal. At. Spectrom. 26, 425–430.

Huang, H.Q., Li, X.H., Li, W.X., Li, Z.X., 2011. Formation of high $\delta^{18}O$ fayalite-bearing A-type granite by high-temperature melting of granulitic metasedimentary rocks, southern China. Geology 39, 903–906.

Jackson, S.E., Pearson, N.J., Griffin, W.L., Belousova, E.A., 2004. The application of laser ablation-inductively coupled plasma-mass spectrometry to *in situ* U-Pb zircon geochronology. Chem. Geol. 211, 47–69.

Jiang, S.Y., Yu, J.M., Lu, J.J., 2004. Trace and rare-earth element geochemistry in tourmaline and cassiterite from the Yunlong tin deposit, Yunnan, China: Implication for migmatitic-hydrothermal fluid evolution and ore genesis. Chem. Geol. 209, 193–213.

Jiang, Y.H., Jiang, S.Y., Zhao, K.D., Ling, H.F., 2006. Petrogenesis of Late Jurassic Qianlishan granites and mafic dykes, Southeast China: Implications for a back-arc extension setting. Geol. Mag. 143, 457–474.

Jiang, Y.H., Jiang, S.Y., Dai, B.Z., Liao, S.Y., Zhao, K.D., Ling, H.F., 2009. Middle to late Jurassic felsic and mafic magmatism in southern Hunan Province, Southeast China: Implications for a continental arc to rifting. Lithos 107, 185–204.

Kempe, U., Belyatsky, B., Krymsky, R., Kremenetsky, A., Ivanov, P., 2001. Sm-Nd and Sr isotope systematics of scheelite from the giant Au (-W) deposit Muruntau (Uzbekistan): Implications for the age and sources of Au mineralization. Mineral. Deposita 36, 379–392.

Koppers, A.A., 2002. ArArCALC–software for $^{40}Ar/^{39}Ar$ age calculations. Comput. Geosci. 28, 605–619.

Liu, Y.P., Li, Z.X., Li, H.M., Guo, L.G., Xu, W., Ye, L., Li, C.Y., Pi, D.H., 2007. U-Pb geochronology of cassiterite and zircon from the Dulong Sn-Zn deposit: Evidence for cretaceous large-scale granitic magmatism and mineralization events in southeastern Yunnan province, China. Acta Petrol. Sin. 23, 967–976 (in Chinese with English abstract).

Liu, Y.S., Gao, S., Hu, Z.C., Gao, C.G., Zong, K.Q., Wang, D.B., 2010a. Continental and oceanic crust recycling-induced melt-peridotite interactions in the Trans-North China Orogen: U-Pb dating, Hf isotopes and trace elements in zircons from mantle xenoliths. J. Petrol. 51, 537–571.

Liu, Y.S., Hu, Z.C., Zong, K.Q., Gao, C.G., Gao, S., Xu, J., Chen, H.H., 2010b. Reappraisement and refinement of zircon U-Pb isotope and trace element analyses by LA-ICP-MS. Chin. Sci. Bull. 55, 1535–1546.

Lu, J.J., Zhang, R.Q., Wang, R.C., 2011. Two contrasting ore-bearing granites: Sn-bearing Qitianling granite and W-bearing Xintianling granite, Hunan province. Mineral. Mag. 75, 1359.

Lu, J.J., Wang, R.C., Ma, D.S., Chen, W.F., Xie, L., Zhang, R.Q., 2012. Two contrasting Sn- and W-bearing granites in the Nanling Range, South China: Evidence from Hf isotopes. Mineral. Mag. 76, 2036.

Ludwig, K.R., 2003. User's manual for Isoplot/Ex version 3.00: A geochronology toolkit for microsoft excel, No. 4. Berkeley Geochronological Center, Special Publication.

Luo, J.C., Hu, R.Z., Fayek, M., Li, C.S., Bi, X.W., Abdu, Y., Chen, Y.W., 2014. In-situ SIMS uraninite U-Pb dating and genesis of the Xianshi granite-hosted uranium deposit, South China. Ore Geol. Rev. http://dx.doi.org/10.1016/j.oregeorev.2014.06.016.

Mao, J.W., Chen, Y.C., Bi, C.S., Li, H.Y., 1995. Geology of tin deposits in China. Sci. Geol. Sin. 4, 121–177.

Mao, J.W., Wang, Y.T., Lehmann, B., Yu, J.J., Du, A.D., Mei, Y.X., Li, Y.F., Zang, W.S., Stein, H.J., Zhou, T.F., 2006a. Molybdenite Re-Os and albite $^{40}Ar/^{39}Ar$ dating of Cu-Au-Mo and magnetite porphyry systems in the Yangtze River valley and metallogenic implications. Ore Geol. Rev. 29, 307–324.

Mao, J.W., Xie, G.Q., Li, X.F., Zhang, C.Q., Wang, Y.T., 2006b. Mesozoic large-scale mineralization and multiple lithospheric extensions in South China. Acta Geological Sinica-English Edition 80, 420–431.

Mao, J.W., Cheng, Y.B., Chen, M.H., Pirajno, F., 2013. Major types and time-space distribution of Mesozoic ore deposits in South China and their geodynamic settings. Mineral. Deposita 48, 267–294.

Peng, J.T., Zhou, M.F., Hu, R.Z., Shen, N.P., Yuan, S.D., Bi, X.W., Du, A.D., Qu, W.J., 2006. Precise molybdenite Re-Os and mica Ar-Ar dating of the Mesozoic Yaogangxian tungsten deposit, central Nanling district, South China. Mineral. Deposita 41, 661–669.

Qu, W.J., Du, A.D., 2003. Highly precise Re-Os dating of molybdenite by ICP-MS with Carius tube sample digestion. Rock Miner. Anal. 22, 254–257 (in Chinese with English abstract).

Romer, R.L., Lüders, V., 2006. Direct dating of hydrothermal W mineralization: U-Pb age for hübnerite ($MnWO_4$) Sweet Home Mine, Colorado. Geochim. Cosmochim. Acta 70, 4725–4733.

Romer, R.L., Smeds, S.A., 1994. Implications of U-Pb ages of columbite-tantalites from granitic pegmatites for the Palaeoproterozoic accretion of 1.90-1.85 Ga magmatic arcs to the Baltic Shield. Precambrian Res. 67, 141–158.

Romer, R.L., Wright, J.E., 1992. U-Pb dating of columbites: A geochronologic tool to date magmatism and ore deposits. Geochim. Cosmochim. Acta 56, 2137–2142.

Romer, R.L., Smeds, S.A., Černý, P., 1996. Crystal-chemical and genetic controls of U-Pb systematics of columbite-tantalite. Mineral. Petrol. 57, 243–260.

Selby, D., Creaser, R.A., 2001. Re-Os geochronology and systematics in molybdenite from the Endako porphyry molybdenum deposit, British Columbia, Canada. Econ. Geol. 96, 197–204.

Selby, D., Creaser, R.A., Hart, C.J.R., Rombach, C.S., Thompson, J.F.H., Smith, M.T., Bakke, A.A., Goldfarb, R.J., 2002. Absolute timing of sulfide and gold mineralization: A comparison of Re-Os molybdenite and Ar-Ar mica methods from the Tintina Gold Belt, Alaska. Geology 30, 791–794.

Shirey, S.B., Walker, R.J., 1995. Carius tube digestion for low-blank rhenium-osmium analysis. Anal. Chem. 67, 2136–2141.

Shu, L.S., 2007. Geological setting of the Nanling Range. In: Zhou, X.M. (Ed.), Genesis of Late Mesozoic granites and lithospheric evolution in the Nanling Range. Science Press, Beijing, pp. 3–22 (in Chinese).

Sláma, J., Košler, J., Condon, D.J., Crowley, J.L., Gerdes, A., Hanchar, J.M., Horstwood, M.S.A., Morris, G.A., Nasdala, L., Norberg, N., Schaltegger, U., Schoene, B., Tubrett, M.N., Whitehouse, M.J., 2008. Plešovice zircon: A new natural reference material for U-Pb and Hf isotopic microanalysis. Chem. Geol. 249, 1–35.

Smoliar, M.I., Walker, R.J., Morgan, J.W., 1996. Re-Os ages of group IIA, IIIA, IVA, and IVB iron meteorites. Science 271, 1099–1102.

Snee, L.W., Sutter, J.F., Kelly, W.C., 1988. Thermochronology of economic mineral deposits: Dating the stages of mineralization at Panasqueira, Portugal, by high-precision $^{40}Ar/^{39}Ar$ age spectrum techniques on muscovite. Econ. Geol. 83, 335–354.

Steiger, R.H., Jäger, E., 1977. Subcommission on geochronology: Convention on the use of decay constants in geo- and cosmochronology. Earth Planet. Sci. Lett. 36, 359–362.

Stein, H.J., Markey, R.J., Morgan, J.W., Hannah, J.L., Schersten, A., 2001. The remarkable Re-Os chronometer in molybdenite: How and why it works. Terra Nova 13, 479–486.

Sun, T., Zhou, X.M., Chen, P.R., Li, H.M., Zhou, H.Y., Wang, Z.C., Shen, W.Z., 2005. Strongly peraluminous granites of Mesozoic in Eastern Nanling Range, southern China: Petrogenesis and implications for tectonics. Sci. China Ser. D Earth Sci. 48, 165–174.

Wang, D.Z., Shu, L.S., 2012. Late Mesozoic basin and range tectonics and related magmatism in Southeast China. Geosci. Front. 3, 109–124.

Wang, Y.J., Fan, W.M., Sun, M., Liang, X.Q., Zhang, Y.H., Peng, T.P., 2007. Geochronological, geochemical and geothermal constraints on petrogenesis of the Indosinian peraluminous granites in the South China Block: A case study in the Hunan Province. Lithos 96, 475–502.

Wang, Z.Q., Chen, B., Ma, X.H., 2014. Petrogenesis of the Late Mesozoic Guposhan composite plutons from the Nanling Range, South China: Implications for W-Sn mineralization. Am. J. Sci. 314, 235–277.

Wei, D.F., Bao, Z.Y., Fu, J.M., Cai, M.H., 2007. Diagenetic and mineralization age of the Hehuaping tin-polymetallic orefield, Hunan province. Acta Geol. Sin. Engli. Ed. 81, 244–252.

Wu, S.N., 2006. Geological characteristics of the Hehuaping tin-polymetallic deposit in Chenzhou, Hunan Province. Min. Resour. Geol. 20, 43–46 (in Chinese with English abstract).

Wu, J., Liang, H.Y., Huang, W.T., Wang, C.L., Sun, W.D., Sun, Y.L., Li, J., Mo, J.H., Wang, X.Z., 2012. Indosinian isotope ages of plutons and deposits in southwestern Miaoershan-Yuechengling, northeastern Guangxi and implications on Indosinian mineralization in South China. Chin. Sci. Bull. 57, 1024–1035.

Xu, K.Q., Sun, N., Wang, D.Z., Hu, S.X., Liu, Y.J., Ji, S.Y., 1982. On the origin and metallogeny of the granites in South China. In: Xu, K.Q. (Ed.), Geology of granites and their metallogenetic relations, Proceeding of International Symposium, Nanjing University. Science Press, Beijing, pp. 1–3 (in Chinese).

Yao, Y., Chen, J., Lu, J.J., Wang, R.C., Zhang, R.Q., 2014. Geology and genesis of the Hehuaping magnesian skarn-type cassiterite-sulfide deposit, Hunan Province, Southern China. Ore Geol. Rev. 58, 163–184.

York, D., 1969. Least squares fitting of a straight line with correlated errors. Earth Planet. Sci. Lett. 5, 320–324.

Yuan, H.L., Gao, S., Liu, X.M., Li, H.M., Gunther, D., Wu, F.Y., 2004. Accurate U-Pb age and trace element determinations of zircon by laser ablation-inductively coupled plasma-mass spectrometry. Geostand. Geoanal. Res. 28, 353–370.

Yuan, S.D., Peng, J.T., Hu, R.Z., Li, H.M., Shen, N.P., Zhang, D.L., 2008. A precise U-Pb age on cassiterite from the Xianghualing tin-polymetallic deposit., Hunan, South China. Mineral. Deposita 43, 375–382.

Yuan, S.D., Peng, J.T., Hao, S., Li, H.M., Geng, J.Z., Zhang, D.L., 2011. In situ LA-MC-ICP-MS and ID-TIMS U-Pb geochronology of cassiterite in the giant Furong tin deposit, Hunan Province, South China: New constraints on the timing of tin-polymetallic mineralization. Ore Geol. Rev. 43, 235–242.

Zhao, K.D., Jiang, S.Y., Zhu, J.C., Li, L., Dai, B.Z., Jiang, Y.H., Ling, H.F., 2010. Hf isotopic composition of zircons from the Huashan-Guposhan intrusive complex and their mafic enclaves in northeastern Guangxi: Implication for petrogenesis. Chin. Sci. Bull. 55, 509–519.

Zhao, K.D., Jiang, S.Y., Yang, S.Y., Dai, B.Z., Lu, J.J., 2012. Mineral chemistry, trace elements and Sr-Nd-Hf isotope geochemistry and petrogenesis of Cailing and Furong granites and mafic enclaves from the Qitianling batholith in the Shi-Hang zone, South China. Gondwana Res. 22, 310–324.

Zheng, J.H., Guo, C.L., 2012. Geochronology, geochemistry and zircon Hf isotopes of the Wangxianling granitic intrusion in South Hunan Province and its geological significance. Acta Petrol. Sin. 28, 75–90 (in Chinese with English abstract).

Zhou, X.M., Sun, T., Shen, W.Z., Shu, L.S., Niu, Y.L., 2006. Petrogenesis of Mesozoic granitoids and volcanic rocks in South China: A response to tectonic evolution. Episodes 29, 26–33.

Zhou, Y., Liang, X.Q., Liang, X.R., Wu, S.C., Jiang, Y., Wen, S.N., Cai, Y.F., 2013. Geochronology and geochemical characteristics of the Xitian tungsten-tin-bearing A-type granites, Hunan Province, China. Geotecton. Metallog. 37, 511–529 (in Chinese with English abstract).

Zhu, J.C., Chen, J., Wang, R.C., Lu, J.J., Xie, L., 2008. Early Yanshanian NE trending Sn/W-bearing A-type granites in the western-middle part of the Nanling Mts region. Geol. J. China Univ. 14, 16–21 (in Chinese with English abstract).

Zhu, J.C., Wang, R.C., Lu, J.J., Zhang, W.L., 2010. On the time span between emplacement age and zircon U-Pb age of the Mesozoic granites in Nanling Range, South China: A discussion with Prof. Zhang Bangtong et al. Geol. J. China Univ. 16, 119–123 (in Chinese with English abstract).

Zou, X.W., Cui, S., Qu, W.J., Bai, Y.S., Chen, X.Q., 2009. Re-Os isotope dating of the Liguifu tungsten-tin polymetallic deposit in Dupangling area, Guangxi. Geol. China 36, 837–844 (in Chinese with English abstract).